

UC Riverside

UC Riverside Previously Published Works

Title

NMR-Guided Design of Potent and Selective EphA4 Agonistic Ligands

Permalink

<https://escholarship.org/uc/item/6wz125t2>

Journal

Journal of Medicinal Chemistry, 64(15)

ISSN

0022-2623

Authors

Baggio, Carlo

Kulinich, Anna

Dennys, Cassandra N

et al.

Publication Date

2021-08-12

DOI

10.1021/acs.jmedchem.1c00608

Peer reviewed



Published in final edited form as:

J Med Chem. 2021 August 12; 64(15): 11229–11246. doi:10.1021/acs.jmedchem.1c00608.

NMR-guided design of potent and selective EphA4 agonistic ligands

Carlo Baggio¹, Anna Kulinich¹, Cassandra N. Dennys², Rochelle Rodrigo², Kathrin Meyer², Iryna Ethell¹, Maurizio Pellecchia^{1,*}

¹ Division of Biomedical Sciences, School of Medicine, University of California Riverside, 900 University Avenue, Riverside, CA 92521, USA.

² Nationwide Children's Hospital, 700 Children's Drive, Columbus, OH 43205, USA.

Abstract

In this manuscript we applied an innovative nuclear magnetic resonance (NMR) guided screening and ligand design approach, named focused high throughput screening by NMR (*f*HTS by NMR) to derive potent, low molecular weight ligands capable of mimicking the interactions elicited by the ephrin ligands on the receptor tyrosine kinase EphA4. The agents bind with nanomolar affinity, trigger receptor activation in cellular assays with motor neurons, and provide remarkable motor neuron protection from Amyotrophic Lateral Sclerosis (ALS) patient derived astrocytes. Structural studies on the complex between EphA4 ligand binding domain and a most active agent provide insights on the mechanism of the agents at a molecular lever. Together with preliminary *in vivo* pharmacology studies, the data form a strong foundation for the translation of these agents for the treatment of ALS and potentially other human diseases.

* Corresponding Author: Maurizio.pellecchia@ucr.edu.

Author contributions: MP directed research, designed and conceived the compounds listed in Tables 1–6 with CB, coordinated testing of the molecules, interpreted data and results, and wrote the manuscript. MP and CB also performed modeling studies and prepared all Tables 1–6 and Figures 1–4. CB prepared proteins and mutants, iteratively synthesized all agents listed in the manuscript, and tested each agent by NMR and/or ITC. CB wrote the methods parts relative to these studies. AK under the supervision of IE performed and analyzed the data reported in Figures 5 and 6. CD under the supervision of KM, and the participation of RR, performed the studies relative to Figure 7. The X-ray studies were performed under contract by Proteros USA (Cambridge, MA, USA), while pharmacokinetic studies were performed at the University of California San Diego (San Diego, CA, USA), Center for Drug Discovery Innovation core facility.

Notes: UCR has filed a patent application relative to the agents and their methods of use for ALS and other indications. UCR may license the invention and some or all authors may receive a portion of the eventual royalties, according to standard University of California licensing and royalties sharing policies. Small amounts of any of the agents reported in the manuscript can be made available for research purposes through a standard MTA.

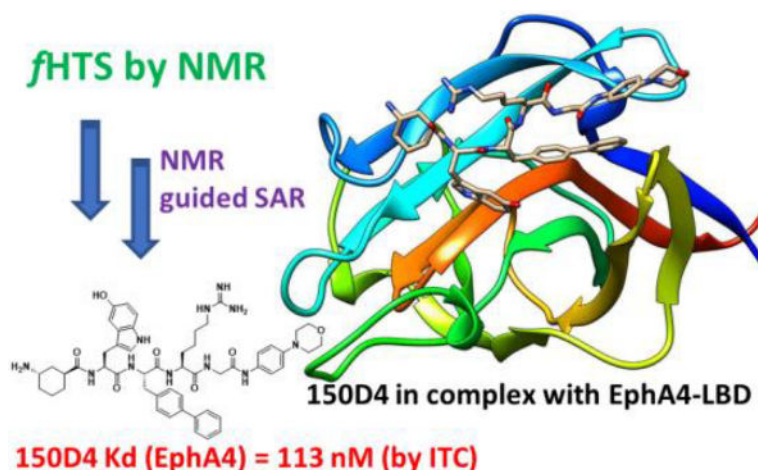
Ancillary information

The coordinates of compound **150D4** in complex with EphA4-LBD have been deposited in the protein data bank (PDB ID 7OFV). Authors will release the atomic coordinates upon article publication.

ASSOCIATED CONTENT

Supporting Information: The Supporting Information is available free of charge on the ACS Publications website. Table S1 reports chemical structures and binding properties of additional EphA4 targeting. Table S2 reports data collection and refinement statistics for the X-ray studies of the complex between EphA4-LBD and **150D4**. Table S3 reports *in vivo* pharmacology studies including PK and brain exposure in mice receiving **150D4**. A molecular formula strings table is also included. Figure S1 reports HPLC traces for tested compounds. Figure S2 describes the general scheme for the synthesis of compounds **150D4** and **32**. Figure S3 describes the general scheme for the synthesis of compounds **31** and **30**. Figure S4 describes the general scheme for the synthesis of compounds listed in Table 1. Figure S5 describes the general scheme for the synthesis of compounds listed in Table 2. Figure S6 describes the general scheme for the synthesis of compounds listed in Table 3. Figure S7 describes the general scheme for the synthesis of compounds listed in Table 4. Figure S8 describes the general scheme for the synthesis of compounds listed in Table 5. Figure S9 reports original uncropped WB images that generated Figure 5. A molecular formula strings file (CSV) for final compounds is also provided.

Graphical Abstract



Keywords

HTS by NMR; fHTS by NMR; PPIs; EphA4; ALS; 150D4

Introduction

Recent studies clearly linked excessive un-ligated EphA4, that can result both by EphA4 overexpression¹ and/or reduced levels of its ephrinA5 ligand,² to the progression of Amyotrophic Lateral Sclerosis (ALS), a degenerative disease that affects motor neurons. These observations suggest that synthetic EphA4 agonistic agents, hence mimicking ephrinA5, could be translated in potentially effective ALS treatments.³ However, the identification of potent and pharmacologically viable agents mimicking EphA4-ephrinA5 interactions (hence a protein-protein interaction, PPI) remains a challenging task. We recently proposed the HTS by NMR approach⁴⁻⁵ that consists of combining principles of positional scanning combinatorial chemistry and protein-based NMR screening to identify, within libraries of > 100,000 compounds, possible initial binders to protein-protein interactions. Briefly, combinatorial libraries of tri- or tetra-peptides (most often including non-natural amino-acids) are assembled in a positional scanning fashion.⁶ In a library of tripeptides, the approach consists of assembling compound mixtures in which systematically each element is fixed at one position while all other possibilities are contained for the two other positions. For example, a library of tripeptides assembled out of 50 (aa₁, ..., aa₅₀) natural and non-natural amino acids will include 50 mixtures aa₁-X-X, ..., aa₅₀-X-X (where X represents all 50 amino acids), 50 mixtures X-aa₁-X, ..., X-aa₅₀-X, and 50 mixtures X-X-aa₁, ..., X-X-aa₅₀. Testing each mixture by sensitive protein-NMR spectroscopy methods⁷ will identify which of the aa₁, ..., aa₅₀ elements would be preferred at each of the 3 positions. Subsequently, synthesis of individual agents presenting the combination of the most active elements at each position would lead to initial hit agents. In our experience, this approach when deployed against PPIs, can result in the identification of initial tri- or tetra-peptides with affinities in the high micromolar range.⁴ Subsequently, structure-based iterative optimizations of the initial hits can lead to more potent and selective agents.^{3, 5}

More recently, we proposed using a “focused” positional scanned library for the approach, in which each element of the library is derivatized with a target specific (or a target class specific) chemical binding moiety. We refer to this method as focused HTS by NMR or *f*HTS by NMR.^{8–9} For example, in metallo-proteins, a focused positional scanning library was derived by introducing a metal chelating group (an hydroxamate) in each element of the combinatorial library.^{8–9} The approach was proven very successful in the rapid identification of ligands with low nanomolar affinities for MMPs.^{8–9} In protein-protein interactions the method can be likewise deployed if a particular amino acid type (or a chemical fragment, or a chemical moiety) is known to be an anchoring binding substructure for the given target. For example, it is known that tetrapeptides binding to the Inhibitor of Apoptosis Protein (IAP) family require an anchoring Ala residue at the N-terminus for binding.¹⁰ Hence, we found that positional scanning libraries in which all elements are derivatized with an *N*-terminal Ala, when screened by NMR against IAP proteins, resulted in the rapid identification of potent nanomolar agents.¹⁰ Hence, here we deployed the *f*HTS by NMR to derive potent and selective agents targeting the ligand binding domain of the receptor tyrosine kinase EphA4.

Recent studies on the role of EphA4 in disease were focused on ALS, where until now SOD1 mutant transgenic mice models have been used to evaluate the potential therapeutic benefit of experimental therapeutics for this specific form of *f*ALS. While deletion of the EphA4 gene (heterozygous) in a SOD1(G93A) mouse model of ALS resulted in improved survival,¹ more recent studies seemed to be contradictory on how and when to target EphA4 in ALS. For example, ubiquitous reduction of EphA4 levels to 50% in the same SOD1(G93A) mice at 60 days of age, did not improve disease onset or survival,¹¹ suggesting that specific knockdown in EphA4 in adulthood may have a limited therapeutic potential for ALS. Moreover, pharmacological inhibition of EphA4 also produced non-conclusive results using transgenic SOD1(G93A) animal models. For example, earlier studies with an EphA4 antagonistic peptide KYL¹² targeting its ligand binding domain similar to APY-d3, apparently improved onset and survival in a rat model for ALS.¹ However, the study also reported a similar *in vivo* effect with a previously identified small molecule pyrrole-salicylate agent¹³ that we and others^{3, 14–15} later recognized to be a false positive, and not targeting EphA4 potently or specifically, perhaps further corroborating the variability of the transgenic models in evaluating the potential efficacy of experimental therapeutics. A more controlled study with the optimized EphA4 antagonist agent APY-d3¹⁶ was also recently reported and the studies concluded there was no difference between treatment groups and controls in disease onset or survival (http://www.ephrins.org/doc/libro_abstract_2018.pdf). More recently, a fusion protein combining the extracellular domain of wild-type EphA4 with an IgG Fc fragment (EphA4-Fc) has been proposed as a decoy to suppress EphA4 signaling, and showed in SOD1(G93A) mice models only a modest improvement in survival but a more significant improvement on delaying disease onset.¹⁷

EphA4 binds to their natural ligands, the ephrins, inducing bidirectional signaling, and the ligands can interact with the receptor in *cis* (i.e from the same cells) or from adjacent cells (i.e. the astrocytes).¹⁸ When EphA4 is aberrantly overexpressed, the unbound receptor can exert a pro-apoptotic activity in motor neurons (MNs),¹⁹ while the ephrin

bound receptor is not pro-apoptotic, suggesting that ephrin-mimetics (or agonistic agents) may be needed to ameliorate MNs cell death induced by overexpression of EphA4 in ALS patients. Accordingly, it was recently found that reduction of ephrin-A5 aggravates disease progression in amyotrophic lateral sclerosis, perhaps because eliminating its ephrin ligand, unbound EphA4 can exert its pro-apoptotic effect in MNs.² These observations collectively would suggest that ephrinA5 mimetics, hence EphA4 agonistic agents, rather than antagonists, or EphA4-decoys, or genetic suppression of EphA4 expression, may provide a benefit for ALS patients. Indeed, we showed previously that *in vivo* administration of agonistic agent 123C4 daily in SOD1(G93A) transgenic mice significantly prolonged survival in the treated cohort.³

On these premises, we deployed the fHTS by NMR to derive novel potent agonistic EphA4 targeting ligands strategy that ultimately resulted in the identification of agents binding with enthalpy driven nanomolar affinity for the EphA4 ligand binding domain, as determined by isothermal titration calorimetry, and act as agonists in neuronal cells. Structural studies by solution NMR spectroscopy and X-ray crystallography, including the high-resolution structure of the complex between the most potent agent and the ligand binding domain of EphA4, also provide molecular determinants for the binding of the agents and their agonistic properties. We report on the detailed studies that led to the identification and optimization of this innovative agent, including its biophysical, biochemical, and pharmacological characterizations.

Results

fHTS by NMR identifications of novel EphA4-Ligand Binding Domain (LBD) ligands

In our previous work, we deployed the HTS by NMR approach against the ligand binding domain of EphA4 by using a tri-peptide positional scanning library consisting of ~ 125,000 agents.⁵ These efforts, and subsequent iterative optimizations of the initial high micromolar affinity ligands, resulted in agent 123C4, with affinity for the isolated EphA4 ligand binding domain (LBD) of ~ 400 nM by isothermal titration calorimetry (ITC).^{3, 5}

Structure activity relationships on agent 123C4 revealed the importance of a small aliphatic *N*-terminal amine, preferably an Ala, a β -Ala, or a GABA residue.³ Hence, based on our previous experience with the fHTS by NMR, we opted to derive and screen a positional scanning library of tetrapeptides, all containing a fixed Ala residue at the N-terminus as an initial anchoring moiety. The library, containing 46 natural and non-natural amino-acids at each of the three scanned positions, spanned a chemical space of nearly 100,000 Ala-XXX compounds, arranged in 138 mixtures (Figure 1).²⁰ Testing and rank ordering of each mixture was accomplished by measuring sensitive ¹H 1D-aliphatic NMR of recombinant EphA4 ligand binding domain (at 20 μ M) and by monitoring eventual chemical shift perturbations induced by each given mixture (at 2 mM total compound concentration). Positive mixtures were therefore identified as those producing a significant perturbation in the aliphatic region of the spectrum (Figure 1), and correspondingly fixed position amino acids were selected at each of the 3 positions of the Ala-XXX tetrapeptides. Remarkably, the screen and subsequent synthesis and testing of the best combination agent, identified compound **1** with K_d in the low micromolar range as determined by ITC (Figure 1).

Hence, unlike the HTS by NMR approach, in which initial hit molecules presented K_d values for EphA4-LBD in the triple-digit micromolar range,⁵ the \mathcal{H} TS by NMR delivered an agent with single digit micromolar affinity, therefore more directly amenable to further hit-to-lead optimization, as reported below.

Structure-activity relationship studies aimed at hit-to-lead optimizations

An efficient strategy to monitor ligand binding by protein NMR is the production of protein samples that are uniformly labeled with $^{13}\text{C}^e$ -methionine.³ 2D [^{13}C , ^1H] correlation NMR spectra measured with such protein targets, collected in absence or presence of test ligands can be used to monitor ligand binding and make, albeit qualitative, determinations on possible conformational changes induced by test ligands on the protein target. For example, residues Met 164 and Met 60 are located within the binding site of the EphA4-LBD, in the D-E loop and J-K loop, respectively (Figure 2A, B). Hence, Met $^{13}\text{C}^e$, $^1\text{H}^e$ chemical shift perturbations induced by test ligands can be used to monitor and iteratively rank order ligands' binding as illustrated in Figure 2. The specific resonance assignments of these Met residues have been obtained previously by single point mutations followed by $^{13}\text{C}^e$ -methionine labeling and NMR analysis.³ In targeting EphA4, an important aspect regarding the activity of its ligands is whether these agents could be predicted to work as antagonists or agonists. Our previous studies identified 123C4 as a possible agonistic agent,³ while antagonistic compounds have been recently derived by phage display strategies, represented by the 13mer cyclic peptide APY-d3 as the most potent agent reported to date targeting EphA4-LBD (Figure 2).¹⁶ Not surprisingly, comparison of the structures of EphA4-LBD bound to ephrinA5 (a natural EphA4 agonistic ligand) versus EphA4-LBD bound to antagonist APY-d3, revealed differences in the conformational changes induced by the two ligands. Most notably, loop G-H, containing residue Met 115 and located at the EphA4-LBD dimerization interface, assumes two different conformations in the agonist versus antagonist bound structures (Figure 2A,B). Hence, chemical shift perturbations induced by test ligands to the resonances of Met 115 can be also used to anticipate, albeit qualitatively, whether a ligand caused conformational changes similar to those induced by an agonist or by an antagonist (Figure 2C). Conversely, structural studies suggest that agonistic agents open the ligand binding domain and cause a large conformational change in the J-K loop, composed of Met 164. Hence, we expect that antagonists will cause larger chemical shift perturbations of Met 115, while agonists would display larger changes in Met 164, as we observed in Figure 2C. Met 60 chemical shift changes can be more directly attributed to direct interactions of the ligand with the residue and to some extent also perhaps to some expected locally induced conformational changes. On the contrary, and as mentioned above, large chemical shift changes for the resonances of residues Met 115 or Met 164 correlated to binding to antagonist agent APY-d3, or by agonistic agent 123C4, respectively. Hence, during the optimizations we monitored the chemical shifts of these residues to anticipate whether the test agent would cause conformational changes that are more similar to those caused by the antagonist or by the agonist. Therefore, in carrying out stepwise, iterative structure-activity relationship optimizations studies on initial compound **1**, we used 2D [^{13}C , ^1H] correlation spectra with $^{13}\text{C}^e$ -Met-labeled EphA4-LBD to make such qualitative determinations, while we relied on ITC measurements for quantitative determinations of the thermodynamics of binding and of the dissociation constants. We firmly believe that

it was necessary to use these robust biophysical approaches to iteratively gather detailed information on the binding properties of the agents during the optimization steps, given that biochemical assays have produced false positive agents in the field in the past.^{3, 14}

Hence, and based on our HTS by SAR strategy, following the identification of agent **1** (Figure 1), we designed, synthesized, and tested several agents aimed at optimizing each substructure independently. First, the *N*-terminal Ala position was replaced by other aliphatic amines, also taking into account our previous SAR studies with 123C4.³ These studies are summarized in Table 1 that reports K_d measurements by ITC along with ligand induced chemical shifts perturbations on residue Met 164. Of note is that none of the novel agents perturbed Met 115 chemical shifts, suggesting that the series is behaving more like 123C4, hence agonistic, rather than the antagonistic APY-d3.

Replacement of the *N*-terminal Ala with longer aliphatic chains such as γ -aminobutyric acid (compound **3**) increased the affinity of the agent for EphA4 to the sub-micromolar range. Further SAR studies at the same position were also carried out with agents containing a 5 hydroxy tryptophan in P2, given that it was previously found that such substitution resulted in agents with improved binding affinity (i.e. comparing agent **3**, Table 1, with **4** Table 2). These efforts identified either the γ -aminobutyric acid (compound **4**) or (1S,3S)-3-aminocyclohexane-1-carboxylic acid (compound **6**) as possible preferred replacements of the Ala residue in the P1 position. Compound **6** is particularly interesting based on the larger NMR chemical shifts induced on the resonances of Met 164 and, based on the reduced losses on entropy upon binding, suggesting the perhaps the constrained cyclohexyl moiety more effectively juxtaposes the primary ammine with its binding counterpart.

Further attempts to optimize compound **4** by introducing small modifications of the P2 5OH-Trp residue did not result in agents with improved affinity (Table 2).

Hence, we focused on systematic, stepwise optimizations of other positions, starting with replacements of the P3 phenyl-Phe residue as reported in Table 3. Replacing the P3 position with a α -naphthyl-Ala (compound **12**) or a β -naphthyl-Ala (compound **13**) reduced the affinity significantly, while smaller substitutions on the biphenyl ring of compound **4** were more tolerated, and in some instances resulted in agents with improved binding affinity for EphA4-LBD (i.e. compounds **16** and **17**).

Likewise, the role of h-Arg in P4 was probed by synthesizing and testing agents with various positively charged residues as listed in Table 4. These efforts suggest that replacements of the D-hArg are more tolerated as typified by agents **21** or **22** containing L-Arg or L-Lys in that position. These limited SAR studies in P4 suggest that perhaps this residue is not intimately in direct contact with EphA4-LBD, as also corroborated by the relatively flat results for the HTS by NMR in P4 that did not identify a clearly preferred amino acid at that position over others (Figure 1).

Hence, keeping as an upper limit of the molecular weight of the final agents less than 1000 Da,²¹ and following our previous optimization strategies, we opted to probe whether the binding affinity of the agents could be further improved by elongating the molecules with

one additional P5 element. Interestingly, only derivatization with Gly or D-Ala resulted in agents with similar or slightly improved affinity, while elongation with other amino acids resulted in agents with significantly reduced affinity (supplementary Table S1).

Therefore, fixing Gly at the N-terminus, we further tested whether agents could be further elongated with small amines, again trying to keep the MW within 1000 Da. These efforts are summarized in Table 5, where several aromatic amines were introduced and found to have improved the binding affinity and caused a larger shift of the resonances of Met 164.

Finally, based on the data from Tables 1–5, we synthesized additional agents presenting various combinations of the most active substituents at the P1-P5 positions (Table 6).

Noteworthy is that the resulting agents, all within MW ~ 1000 Da, displayed a binding affinity for EphA4-LBD that is comparable to that of the phage display derived (and extensively optimized) antagonistic cyclic 13mer peptide APY-d3 (MW = 1402; Figure 2; Table 6). Moreover, the agents are very soluble in buffer, that may turn out particularly useful if their administration as therapeutics would require intrathecal delivery.

In summary, the HTS by NMR approach of the Ala-XXX positional scanned tetra-peptide library, followed by stepwise and iterative optimizations of the P1-P4 positions, and the introduction of a P5 amine at the C-terminal, resulted in agents that are as potent as those derived from an extensively optimized phage display derived APY-d3 peptide. Perhaps most importantly, unlike APY-d3, the agents are predicted to work as agonists based on chemical shift perturbations detected via the $^{13}\text{C}^e/{}^1\text{H}^e$ resonances of Met 115, Met 164, and Met 60 (Table 6).

To assess the selectivity of the final agents (Table 6), we tested them against the two most closely related Eph ligand binding domains, namely EphA3 (~ 73% sequence identity with EphA4 within the LBD) and EphA2 (~ 55% sequence identity with EphA4 within the LBD) (Table 6). Under the same experimental conditions, the agents appeared inactive against the EphA2, while displayed micromolar affinities (at best) against the EphA3. Hence the agents are > ten-fold selective for the EphA4 compared to its most closely related receptor, the EphA3 (Table 6). These data identified compound **33** (named **150D4**; Table 6) as a new lead agonistic agent targeting EphA4.

Molecular basis for the affinity and the selectivity of 150D4 for EphA4-LBD

To further investigate at the molecular level the basis of binding and selectivity of most potent agent, in addition to the solution NMR spectroscopy studies as described above, we obtained the high-resolution X-ray structure of the complex between EphA4-LBD and **150D4**.

As mentioned, sequence specific resonance assignments of the Met residues have been obtained in our previous studies by single point mutations followed by $^{13}\text{C}^e$ -methionine labeling and NMR analysis.³ Chemical shifts perturbations upon ligand titration to the $^{13}\text{C}^e$ -Met labeled EphA4-LBD occurred in slow-exchange in the NMR-time scale, that is upon titration of **150D4** the cross-peaks corresponding to both $^{13}\text{C}^e/{}^1\text{H}^e$ resonances of Met

60 and Met 164 progressively disappeared, while two new cross-peaks appeared, which is typical of tight binding affinities.⁷ Two methionine residues, Met 164 and Met 60, are located in the ephrin binding site of EphA4-LBD, while small or no significant perturbations are observed for residue Met 115, in the G-H loop at the dimerization interface in the ephrin-bound structures (Figure 3). Chemical shifts differences of Met 60 resonances between the free versus **150D4** bound form provide an estimated upper limit for the off rate for the complex of $k_{\text{off}} < 60 \text{ s}^{-1}$, that assuming a diffusion limited on rate of $10^9 \text{ M}^{-1} \text{ s}^{-1}$, would correspond to a dissociation constant $K_d < 60 \text{ nM}$ (Figure 3B), thus in good agreement with the ITC data, that indicated a K_d of 113 nM for **150D4** versus EphA4-LBD. On the contrary limited binding was observed in a similar assay against EphA3 or EphA2 (Figure 3A).

Furthermore, and in agreement with our binding and NMR data, we found that **150D4** efficiently displaces the binding of ephrinA5 (the most potent endogenous ephrin ligand for EphA4)²² using displacement 2D [¹³C, ¹H] correlation spectra (Figure 3D).

Next, we determined the X-ray structure of EphA4-LBD in complex with **150D4** at 1.43 Å resolution (Figure 4). The crystals contained one monomer of EphA4-LBD in the asymmetric unit comprising EphA4-LBD residues Asn 29 to Arg 209 and the ligand. The structure of the ligand binding domain of EphA4-LBD in complex with ligand **150D4** adopts a typical bi-lobal architecture that is characteristic of other members of the eukaryotic protein kinase family (Figure 4). The resulting electron density showed an unambiguous binding mode for the ligand **150D4**, including the orientation and conformation of the ligand. Based on a distance of less than 3.5 Å of the donor and acceptor atoms we could identify several specific hydrogen bonds of the ligand **150D4**, namely to the main chain atoms of Ile 192 and Met 60 as well as the side chain atoms of Glu 55 and Gln 71. According to the above distance criteria we could also identify the presence of additional hydrophilic interactions to the main chain atoms of Met 60 as well as the side chain atoms of Thr 104 and Arg 162. The following residues can be found in the vicinity of the ligand with a maximum distance of 3.9 Å (Figure 4): Glu 55, Ile 59, Met 60, Asp 61, Glu 62, Gln 71, Val 72, Cys 73, Thr 104, Leu 105, Arg 106, Ile 159, Met 164, Cys 191, Ile 192, and Ala 193.

Several of such structural details of the binding mode of **150D4** can fully explain the observed SAR studies of Tables 1–5. For example, the *N*-terminal amine is involved in hydrogen bonding with EphA4 Glu 55, the tryptophan in position P2 occupies a shallow hydrophobic sub pocket, with the 5-hydroxyl group involved in hydrogen bonding with Arg 106 mediated by a water molecule, the bi-phenyl group of position P3 occupies a deep pocket, juxtaposing the aromatic rings in proximity of Met 164 (Figure 4). This geometry likely justifies the large perturbations induced by our agents on the chemical shifts of Met 164. The C-terminal portion of the molecule, with the P4 homo-Arg does not seem to be intimately involved intermolecular interactions, in close agreement with our *A*HTS by NMR and SAR data (Figure 1, Table 3), where the P4 position appeared to be less critical for binding. On the contrary, phenyl-morpholino in P5, also conferring increased solubility to the agent, is likely causing the large conformational change in the J-K loop (Figure 4), in agreement with Met 164 NMR chemical shift perturbation studies, presumably further promoting an agonist-like activity of the agent.

In this regard, analysis of the conformations of the loop regions D-E, J-K, and G-H in **150D4** bound EphA4-LBD suggests that these loops adopt a conformation that is more similar to that adopted by the target when bound to the ephrin ligand (PDB ID 2WO1)²² compared to that of antagonist bound APY-d3 (PDB ID 5JR2).¹⁶ In particular, residue Met 115 within loop G-H did not display the large conformational rearrangement as observed in the complex with APY-d3, in agreement with NMR measurements (Figure 4).

The molecular basis for the selectivity of the compound can also be deduced by analyses of the X-ray structure of EphA4 in complex with **150D4** and the X-ray structure of EphA3 in complex with ephrinA5 (PDB ID 4LOP).²³ Comparing EphA4-LBD and EphA3-LBD structures confirmed that there are only few significant differences in the ligand binding regions of these proteins, amounting to 8 mutations. Hence, we prepared a construct representing the ligand binding domain of EphA3 by introducing these 8 mutations and in our EphA4-LBD construct (see experimental session). Isothermal titration calorimetry measurements with **150D4** and this EphA3-LBD chimera indicated that the agent presented a markedly reduced affinity for this construct (Figure 3, Table 6), despite its high similarity with EphA4-LBD (> 95% sequence identity).

Taken together, these structural data strongly suggest that **150D4** and other related agents in Table 6 represent potent and selective binders for EphA4-LBD, that induce conformational changes upon binding that resemble more closely those induced by agonistic agents.

Cellular studies

An indirect measure of agonism by EphA4 ligands can be assessed by monitoring the phosphorylation of its cytosolic kinase domain upon ligand binding. Hence, we isolated primary motor neurons from postnatal day (P) 0-P2 mouse spinal cords of B6.Cg-Tg(Hlx9-GFP)1Tmj/J (Hb9-GFP) mice. Subsequently, cells were treated with ephrinA1-Fc (R&D Systems, #602-A1) or human Fc (R&D Systems, #110-HG) as controls. EphrinA1-Fc needs clustering for maximal agonistic activity, which was accomplished by the incubation with goat anti-human IgG (Jackson ImmunoResearch, #109-005-003) for 1 h at 4°C. At 2 days in vitro (DIV) primary motor neurons were then treated with pre-clustered Fc (2 µg/mL, as negative control), pre-clustered ephrinA1-Fc (2 µg/mL, as positive control), and various agents including antagonist APY-d3, and agents listed in Table 6, namely 123C4, compound **30**, compound **31**, compound **32**, and **150D4**, each at concentrations 1 µM or 10 µM, for 30 min at 37°C under 5% CO₂/10% O₂ atmosphere, and then processed for western blotting. After cell lysis, cells were exposed to protein-A agarose beads (Sigma, #P1406) and anti-EphA4 antibody (Invitrogen, #371600), for 2 h at 4°C, and subsequently boiled in reducing conditions, spun down, and the supernatant was subjected to WB analysis with an anti-phosphotyrosine antibody and re-probed with EphA4 antibody (Figure 5). These data suggest that most agents induced receptor phosphorylation (Figure 5A,B), with **150D4** resulting more significantly active than others (Figure 5C,D). Direct comparison between **150D4** and our previously derived agonistic agent 123C4 (Table 6) in the same assay, also revealed a significant increased phosphorylation induced by the newest compound (Figure 5E).

To further verify agonism in a functional assay, we also monitored growth cone analysis using 2 DIV primary spinal cord motor neurons treated as described above with Fc, ephrinA1-Fc, 1 μM **150D4**, 10 μM **150D4**, 1 μM **150D4** plus ephrinA1-Fc, or 10 μM **150D4** plus ephrinA1-Fc. After images collection (100 images were collected per treatment group), growth cones were assessed based on filamentous (F)-actin labeling and classified into collapsed and growing based on their morphology. The percentage of neurons with collapsed growth cones was determined. Representative images are reported in Figure 6A–D, including statistical analysis based on differences for multiple groups, as assessed by one-way ANOVA followed by Bonferroni's post hoc tests (Figure 6E). In this experimental setting, **150D4** is effective in inducing growth cone collapse similar to the agonistic clustered ligand ephrinA1-Fc (Figure 6), further corroborating the potential agonism induced by the tested agents.

EphA4 has been directly implicated in the progression of ALS in mice models and in human genetic studies. While the mechanisms for onset and progression of ALS remain largely undetermined, astrocytes have been implicated as significant contributors to motor neuron death in both in familial ALS (*fALS*), that is driven by inactivating mutations within the superoxide dismutase 1 (SOD1) gene and that account for less than 2% of all ALS cases,^{24–26} and the more common sporadic form of ALS (*sALS*).^{24–28} Recently, it was shown that astrocytes derived from both patient groups are similarly toxic to motor neurons.²⁹ Hence, a co-culture assay was developed to provide a meaningful and a more general *in vitro* model system to evaluate potential experimental therapeutics for *sALS* and *fALS*. Preliminarily, we probed the ability of agonistic agent **150D4** (at 10 μM) to rescue *sALS* astrocytes-induced motor neuron death, side by side with first generation agent 123C4. The latter resulted active only at higher concentrations in previous studies (in preparation) in the same assay, hence it was tested at the relatively high concentration of 100 μM for comparison purposes only. Both **150D4** and 123C4 (albeit at a much higher concentration) were able to protect mouse motor neurons from iAstrocytes derived from *sALS* patients (Figure 7).³⁰ However, 150D4 was significantly more potent displaying a significant protecting effect already at 10 μM while much higher concentration of earlier generation agent, 123C4, was needed to obtain a similar protection (Figure 7). In our experience with this assay, most agents tested for unrelated targets did not result in any significant protection, making **150D4** potentially a viable lead agent for further drug development studies for ALS therapeutics. Hence, it is worth noting that the agent is a general cytoprotective compound and would therefore find possible therapeutic applications in both *fALS* and *sALS*.

These data collectively suggest that the agents function as EphA4 agonistic ligands *in vitro* and in relevant cellular and functional assays. Hence, we envision that agents such as **150D4** could find immediate applications in disease areas where activation of EphA4 by the ephrin ligands may be beneficial for ALS patients.

Discussion

EphA4 belongs to large family of receptor tyrosine kinases, which together with their ephrin ligands, is involved in bi-directional signaling events that control several cellular processes during development and in disease.¹⁸ The ephrin mediated signaling occur by interactions

with the extracellular Eph ligand binding domain (LBD), which in turn activates intracellular domains including a kinase domain, in addition to a sterile alpha motif (SAM) domain, and a PDZ binding motif that are believed to propagate the cell signaling cascade. In addition to ALS, in recent years EphA4 went under scrutiny for its possible role critical role in several other conditions,³¹ including abnormal blood clotting, spinal cord injury, and Alzheimer's disease (AD), and potentially other diseases.¹⁴

Numerous structural studies identified the molecular determinants for EphA4-LBD/ephrin interactions.²² In addition, several phage display derived short peptide binders (12-mers) that selectively block ephrin ligands from interacting with the EphA4 have been reported,¹² that bind to EphA4-LBD with K_d values in the low micromolar range.^{12, 32} More recently a cyclic peptide termed APY-d3 (Figure 1) was also reported that displayed antagonistic behavior for the receptor, displacing ephrinA5 mediated phosphorylation and growth cone collapse in neuronal cells.³³ More recently, we reported agent 123C4 (Figure 1), a first synthetic agonistic ligand with a dissociation constant for EphA4-LBD of ~ 400 nM, that was derived by a de novo HTS by NMR campaign, testing a library of ~ 100,000 tri-peptides, including non-natural amino acids, followed by SAR studies.³ In cellular assays, 123C4 was found to have agonistic activity for EphA4 in primary cortical neurons, hence, acting similarly to ephrin ligands, induced receptor phosphorylation and growth cone collapse,³ but the molecular determinants at the basis for such activity have not yet been elucidated.

Structure activity relationships studies with 123C4 pointed at the importance of the *N*-terminal amine for anchoring to the receptor. Hence, we decided to carry out a new focused HTS by NMR campaign,^{2, 5, 19} by screening a tetra-peptide library in which each element of the library contained a fixed Ala residue at the N-terminus.²⁰ Recent experiences from our laboratory strongly suggest that testing a focused positional scanning library, obtained by derivatizing an anchoring moiety (Ala in this case), dramatically enhance the likelihood to identify potent agents within the library.^{8-9, 20}

Indeed, the studies led to the identification of the initial hit molecule compound **1** that was able to bind to EphA4-LBD already with low micromolar affinity (Figure 1, Table 1). Iterative optimizations of each of the positions of the tetra peptide (Tables 1-4), including further derivatizations at the C-terminus with a 5th substituent (Table 5), resulted in the design of the final agents reported in Table 6. Potency, selectivity, and solubility of the resulting agents have been the main guiding criteria during the optimization steps keeping the molecular weight well below 1000 Da (Table 6). During each iterative optimization steps, binding was monitored by NMR spectroscopy with ¹³C^e-Met labeled EphA4-LBD and sensitive isothermal titration calorimetry studies, including testing the agents against the most closely related Eph receptors, namely the EphA3, and EphA2, to assess selectivity. These efforts culminated in a series of agents that bind potently and selectively to EphA4-LBD in the nanomolar range, with minimal targeting of EphA3, and non-significant interactions with EphA2 (Table 6).

To further elucidate at the molecular level the basis for the observed activity and selectivity, we also determined the X-ray structure of **150D4** in complex with EphA4-LBD (Figure 4),

where a dense network of favorable intermolecular interactions can be observed that nicely explain the observed SAR, potency, and selectivity.

Recent X-ray crystallography studies with the EphA4 receptor in complex with an ephrin ligand³⁴ suggested that ligand binding to the EphA4 receptor induces a conformational changes in the D-E and J-K loops in EphA4-LBD that favor receptor activation. Similar studies with antagonist APY-d3 reveal instead conformational changes induced at the loop G-H that perhaps could preclude dimer formation, which is believed to be the first step for receptor activation. Interestingly, loop G-H contains residue Met 115, hence we used ¹³C^ε-Met labeled samples of EphA4-LBD to monitor and compare the binding of the antagonist agent APY-d3, and our agents. We found that while both classes of agents caused widespread changes in the chemical shifts of binding site Met residues 60 and 164 (located in the D-E and J-K loops, respectively), only the antagonist caused very large chemical shift perturbations in G-H loop Met 115 resonances, well in agreement with X-ray studies on that complex. At the same time, these observations would suggest that our new agents, similar to 123C4, could act as agonists for the EphA4. Accordingly, the agents acted as agonists towards EphA4 in primary motor neurons, both by activating receptor phosphorylation and by inducing growth cone collapse, similar to ephrinA1-Fc.

To preliminarily evaluate the potential of our newest generation of agonistic agents, we adopted a more disease specific cell-based assay that monitored the cytoprotective ability of test agents in motor neurons, and also assess their ability to rescue motor neuron death induced by sALS patients derived astrocytes.^{29–30} The data clearly suggest that the agents exert a marked cytoprotective activity and can effectively protect motor neurons from sALS derived iAstrocytes (Figure 7), providing a clear path for the development of these agents as ALS therapeutics.

The bidirectional signaling mediated by ephrinA5 and EphA4 offers also other possible therapeutic opportunities. For example, ephrinA5 mimetics, like **150D4**, could find applications also in oncology, including glioma and colon cancers,^{35–37} where ephrinA5 was found to act as a tumor suppressor, interfering with EGFR. Unlike ephrinA5, **150D4** is more selective for the EphA4 subtype, and being a synthetic agent, it is readily available for translation into a therapeutic agent. Moreover, preliminary *in vivo* pharmacology studies suggest that the agent is brain penetrant after intravenous or intraperitoneal administration (supplementary Table S3) hence it could potentially protect motor neurons *in vivo*. Therefore, we are confident that this new series of potent and selective EphA4 agonistic agents and **150D4** in particular, represent powerful and unprecedented pharmacological tools to further evaluate and validate the therapeutic potential of the EphA4 signaling for the onset and progression of ALS and possibly other diseases. Hence, the agent could be deployed for detailed *in vivo* efficacy evaluations in models of ALS and potentially other human diseases, including Alzheimer disease (AD),³⁸ spinal cord injury,³⁹ brain injury,^{40–41} and some type of cancers.^{42–45} In conclusion, we are confident the reported agents and related data form the basis for the immediate development of novel therapeutics.

Experimental Procedures

Chemistry

General: All reagents and solvents were obtained from commercial sources, including the majority of Fmoc-protected amino acids and resins for solid phase synthesis. NMR spectra were used to evaluate the concentration of stock solutions and were recorded on Bruker Avance III 700 MHz equipped with a TCI cryo-probe. High resolution mass spectral data were acquired on an Agilent 6545 Q-TOF LC/MS instrument. RP-HPLC purifications were performed on a JASCO preparative system equipped with a PDA detector and a fraction collector controlled by a ChromNAV system (JASCO) on a XTerra C18 10 μ 10 \times 250 mm (Waters). Purity of tested compounds was assessed by HPLC using an Atlantis T3 3 μ m 4.6 \times 150 mm² column (H₂O/acetonitrile gradient from 5 to 100% in 45 min). All compounds have a purity >95% (Supporting Figure S1). APY-d3 was synthesized by Innopep (San Diego), while all other agents were synthesized in house by standard solid-phase Fmoc peptide synthesis protocols on BAL resin (Supporting Figures S2–S8). Briefly, for each coupling reaction, 3 eq. of Fmoc-AA, 3 eq. of HATU, 3 eq. of OximaPure, and 5 eq. of DIPEA in 1 ml of DMF were used. The coupling reaction was allowed to proceed for 1 h. Fmoc deprotection was performed by treating the resin-bound peptide with 20% piperidine in DMF twice. Peptides were cleaved from Rink amide resin with a cleavage cocktail containing TFA/TIS/water/phenol (94:2:2:2) for 5 h. The cleaving solution was filtered from the resin, evaporated under reduced pressure and the peptides precipitated in Et₂O, centrifuged and dried in high vacuum.

For the synthesis of Fmoc-amino acids that were not commercially available, 1 equivalent of the unprotected amino acid and 3.75 equivalents of Na₂CO₃ were dissolved in tetrahydrofuran (THF)/ H₂O (1:1) and cooled to 0 °C. 1.1 equivalent of Fmoc chloride was dissolved in THF and added dropwise to the mixture. The reaction was stirred for 2 h at 0 °C. The organic solvent was evaporated under reduced pressure and the pH was lowered to 0 using concentrated HCl. The aqueous phase was extracted 3 times with AcOEt and the collected organic phase was dried with Na₂SO₄, filtered, and evaporated. The resulting crude was purified using a CombiFlash Rf (teledyne ISCO) using cyclohexane/ethyl acetate (10–100%). Purity of all tested agents was > 95%.

(1S,3S)-3-amino-N-((S)-1-(((S)-1-(((S)-6-guanidino-1-(2-((4-(morpholinomethyl)phenyl)amino)-2-oxoethyl)amino)-1-oxohexan-2-yl)amino)-3-(2'-methoxy-[1,1'-biphenyl]-4-yl)-1-oxopropan-2-yl)amino)-3-(5-hydroxy-1H-indol-3-yl)-1-oxopropan-2-yl)cyclohexane-1-carboxamide (30): BAL resin

was used as solid-phase support (0.05 mmol scale). Briefly, a BAL resin was loaded using a solution of 4-(Morpholinomethyl)aniline (3 eq.) in DMF added to the reactor and shaken for 30 min, followed by reduction using Sodium triacetoxyborohydride (3 eq., overnight reaction at room temperature). The resin was subsequently filtered, washed three times with DMF, three times with DCM (3x) and again three times with DMF. For the coupling of Fmoc-Glycine on the secondary amine, reaction time was increased to 2 h. Fmoc deprotection and peptide elongation then followed standard procedures described in the general chemistry section. After cleavage, the crude was purified by preparative RP-HPLC

using a XTerra C18 (Waters) and water/acetonitrile gradient (5% to 100%) containing 0.1% TFA. HRMS: calcd 1000.5404 (M+H)⁺; obs 1000.5412 (M+H)⁺, 1022.5217 (M + Na)⁺.

(1S,3S)-N-((S)-1-(((S)-3-([1,1'-biphenyl]-4-yl)-1-(((S)-6-guanidino-1-((2-((4-morpholinomethyl)phenyl)amino)-2-oxoethyl)amino)-1-oxohexan-2-yl)amino)-1-oxopropan-2-yl)amino)-3-(5-hydroxy-1H-indol-3-yl)-1-oxopropan-2-yl)-3-aminocyclohexane-1-carboxamide (31).: BAL resin was used as solid-phase support (0.05 mmol scale), and the previously described conditions for compound **30** were used to obtain the peptidic part of the agent. After cleavage, the crude was purified by preparative RP-HPLC using a XTerra C18 (Waters) and water/acetonitrile gradient (5% to 100%) containing 0.1% TFA. HRMS: calcd 970.5298 (M+H)⁺; obs 970.5301 (M+H)⁺, 992.5093 (M + Na)⁺.

(1S,3S)-3-amino-N-((S)-1-(((S)-1-(((S)-6-guanidino-1-((2-((4-morpholinophenyl)amino)-2-oxoethyl)amino)-1-oxohexan-2-yl)amino)-3-(2'-methoxy-[1,1'-biphenyl]-4-yl)-1-oxopropan-2-yl)amino)-3-(5-hydroxy-1H-indol-3-yl)-1-oxopropan-2-yl)cyclohexane-1-carboxamide (32).: BAL resin was used as solid-phase support (0.05 mmol scale), and the previously described conditions for compound **150D4** were used to obtain the peptidic part of the agent. After cleavage, the crude was purified by preparative RP-HPLC using a XTerra C18 (Waters) and water/acetonitrile gradient (5% to 100%) containing 0.1% TFA. HRMS: calcd 986.5246 (M+H)⁺; obs 986.5264 (M+H)⁺, 1008.5056 (M + Na)⁺.

1S,3S)-N-((S)-1-(((S)-3-([1,1'-biphenyl]-4-yl)-1-(((S)-6-guanidino-1-((2-((4-morpholinophenyl)amino)-2-oxoethyl)amino)-1-oxohexan-2-yl)amino)-1-oxopropan-2-yl)amino)-3-(5-hydroxy-1H-indol-3-yl)-1-oxopropan-2-yl)-3-aminocyclohexane-1-carboxamide (33) (150D4).: BAL resin was used as solid-phase support (0.05 mmol scale). Briefly, a BAL resin was loaded using a solution of 4-Morpholinoaniline (3 eq.) in DMF added to the reactor and shaken for 30 min, followed by reduction using Sodium triacetoxyborohydride (3 eq., overnight reaction at room temperature). The resin was subsequently filtered, washed three times with DMF, three times with DCM (3x) and again three times with DMF. For the coupling of Fmoc-Glycine on the secondary amine reaction time was increased to 2 h. Fmoc deprotection and peptide elongation then followed standard procedures described in the general chemistry section. After cleavage, the crude was purified by preparative RP-HPLC using a XTerra C18 (Waters) and water/acetonitrile gradient (5% to 100%) containing 0.1% TFA. HRMS: calcd 956.5140 (M+H)⁺; obs 956.5151 (M + H)⁺, 978.4939 (M + Na)⁺.

Protein Expression and Purification—cDNA fragments encoding the ligand binding domain of EphA4 (residues 29–209) cloned into a pET15b vector with the Cysteine 204 mutated to Alanine for stability and an *N*-terminal His tag were used in the expressions of EphA4-LBD. The fragments were transformed into *Rosetta-Gami B(DE3)* competent cells and grown in LB medium at 37 °C with 100 µg/mL of ampicillin until reaching an OD₆₀₀ of 0.6–0.7 followed by induction with 0.4 mM IPTG overnight at 20 °C. Bacteria were then collected by centrifugation and lysed by sonication at 4 °C. Proteins were purified using Ni²⁺ affinity chromatography, eluted in 25 mM Tris at pH 7.5, 500 mM NaCl, and 500

mM imidazole. Finally, the protein was further purified, and buffer exchanged, through a size-exclusion chromatography with a HiLoad 26/ 60 Superdex 75 preparative-grade column into an aqueous buffer composed of 25 mM Tris at pH 7.5, 150 mM NaCl. EphA4 LBD with $^{13}\text{C}^e/^{1}\text{H}^e$ -Met labeled was expressed like previously described but adding a suspension of 100 mg of $^{13}\text{C}^e/^{1}\text{H}^e$ -Methionine in 1 mL of DMSO per liter of LB medium, 10 minutes before induction. EphA3 chimera was produced by introduction the following mutations in EphA4-LBD (29 – 209): Arg37Lys, Gly52His, Ile59Gly, Met60Val, Glu77Asp, Val157Met, Ile159Leu, Met164Leu, Cys204Ala. Transformation, expression, and purification of EphA3-LBD chimera was performed as described above for EphA4-LBD.

For the expression of EphA2-LBD, a pET15b vector encoding for the EphA2 ligand binding domain (residues 27–200) and an *N*-terminal His tag was transformed into Origami(DE3) competent cells. The transformed cells were transferred to LB medium at 37°C with 100 µg/L of ampicillin until reaching an OD₆₀₀ of 0.6–0.7, followed by induction with 0.5 mM IPTG overnight at 20 °C. Bacteria were collected and lysed by sonication at 4°C. The overexpressed protein was purified using Ni²⁺ affinity chromatography and further purified and buffer exchanged through a size-exclusion chromatography with a HiLoad 26/ 60 Superdex 75 preparative-grade column into an aqueous buffer composed of 25 mM Tris at pH 7.5, 150 mM NaCl. Human Ephrin-A5 was obtained from Sino Biological US Inc (Chesterbrook, PA).

Isothermal Titration Calorimetry Measurements—Isothermal titration calorimetry measurements were performed using the Affinity ITC Autosampler from TA Instruments (New Castle, DE). The titrations were performed in a reverse fashion by titrating the protein into the ligand solution. All the measurements were performed at 25°C dissolving the agents in 25 mM Tris at pH 7.5, 150 mM NaCl, and a final DMSO concentration of 1%. The syringe was filled with a 100 µM solution of EphA4-LBD, EphA3-LBD Chimera, or EphA2-LBD, and 20 injections of 2.5 µL each were performed into the cell containing a 20 µM solution of the compounds. The injections were made at 200s or 400s intervals with a stirring speed of 75 rpm. All the solutions were kept in the autosampler at 4°C. The analysis of the thermodynamics signatures and for dissociation constant determination was performed by the NanoAnalyze software (TA Instruments, New Castle, DE) and subsequently exported into Microsoft Excel.

Nuclear Magnetic Resonance Spectroscopy—NMR spectra were acquired on Bruker Avance III 700MHz spectrometer equipped with a TCI cryoprobe. All NMR data were processed and analyzed using TOPSPIN 3.6.1 (Bruker, Billerica, MA, USA). 2D- $^{13}\text{C}, ^1\text{H}$ -HSQC experiments were acquired with 20 µM proteins using 8 scans with 2,048 and 256 complex data points in the ^1H and ^{15}N dimensions, respectively, at 298 K. For the **150D4** NMR titrations in Figure 3 2D- $^{13}\text{C}, ^1\text{H}$ -HSQC experiments were acquired using 16 scans per increment, and for ephrinA5 binding studies (Figure 3) with 10 µM protein, using 32 scans per increment.

For the *HTS* by NMR screening, each of the 138 mixtures (3 × 46) was dissolved into a 5 mm NMR tube to a final concentration of 2 mM in the presence of 20 µM of EphA4-LBD in a buffer containing 25 mM TRIS pH = 7.5, 150 mM NaCl. For each mixture 2D $^{13}\text{C}, ^1\text{H}$

HSQC and 1D ^1H -aliph experiments were acquired. For ranking purposes (Figure 1) a total chemical shift perturbation generated by each mixtures to the 5 peaks below 0 ppm in the 1D ^1H -aliph spectra of EphA4-LBD were considered.

Chemical shift changes (δ) in the 2D [^{13}C , ^1H] spectra were calculated as weight average perturbations observed in the ^1H and ^{13}C dimensions using the following Equation:

$$\Delta\delta = \sqrt{\frac{1}{2} * [(\Delta^1H)^2 + (0.3 * \Delta^{13}C)^2]}$$

Molecular Modeling—Molecular models were analyzed using MOE 2019.0101 (Chemical Computing Group) or Chimera (<http://www.cgl.ucsf.edu/chimera>). Structural comparisons were carried out between the X-ray structure of **150D4** in complex with EphA4-LBD and the structures of the complexes between EphA4 and APY-D3 (PDB-ID 5JR2), EphA4-ephrinA5 (PDB-ID 4BKA), and apo Eph4-LBD (PDB-ID 2WO1).

X-ray Structure Determination—EphA4-LBD was used in crystallisation trials employing both a standard screen with approximately 1200 different conditions, as well as crystallisation conditions identified using literature data. Conditions initially obtained have been optimised using standard strategies, systematically varying parameters critically influencing crystallisation, such as temperature, protein concentration, drop ratio, and others. These conditions were also refined by systematically varying pH or precipitant concentrations. A cryo-protocol was established using PROTEROS Standard Protocols. Crystals have been flash-frozen and measured at a temperature of 100 K. The X-ray diffraction data have been collected from complex crystals of EphA4-LBD mutant C204A with the ligand **150D4** at the Deutsches Elektronen-Synchrotron (DESY, Hamburg, Germany) using cryogenic conditions. The crystals belong to space group P 43 21 2. Data were processed using the programmes autoPROC, XDS and autoPROC, AIMLESS. The phase information necessary to determine and analyze the structure was obtained by molecular replacement. Model building and refinement was performed according to standard protocols with COOT and the software package CCP4, respectively. For the calculation of the free R-factor, a measure to cross-validate the correctness of the final model, about 4.9 % of measured reflections were excluded from the refinement procedure (see supplementary Table S2). Anisotropic B-factor refinement (using REFMAC5, CCP4) has been carried out, which resulted in lower R-factors and higher quality of the electron density map. The ligand parameterization and generation of the corresponding library files were carried out with CORINA. The water model was built with the “Find waters”-algorithm of COOT by putting water molecules in peaks of the Fo-Fc map contoured at 3.0 followed by refinement with REFMAC5 and checking all waters with the validation tool of COOT. The criteria for the list of suspicious waters were: B-factor greater 80 Å², 2Fo-Fc map less than 1.2 σ , distance to closest contact less than 2.3 Å or more than 3.5 Å. The suspicious water molecules and those in the ligand binding site (distance to ligand less than 10 Å) were checked manually. The Ramachandran Plot of the final model shows 90.3 % of all residues in the most favored region, 9.1 % in the additionally allowed region, and 0.6 % in the generously allowed region.

No residues are found in the disallowed region. Statistics of the final structure and the refinement process are listed in supplementary Table S2.

Animal Studies—Primary motor neurons were isolated from spinal cords of B6.Cg-Tg(Hlxb9-GFP)1Tmj/J (Hb9-GFP) mice at postnatal day (P) 0–2. Tissues were dissected, cut into 1–2 mm pieces and treated with a papain/DNase I (0.1 M PBS/0.1% BSA/ 25 mM glucose/5% papain/1×DNase I [Sigma, #D5025–15K]) solution for 20 min at 37°C. Cells were mechanically dissociated, filtered using a 100 µm cell strainer and further purified using OptiPrep gradient centrifugation as described in (Wang, 2017). Neurons were plated on poly-D-lysine (0.5 mg/mL) and laminin (5 µg/mL) coated 6- or 24-well plates (350,000 cells per well of 6-well plate and 75,000 cells per well of 24-well plate) in Neurobasal media with 25 mM glutamine, 1% penicillin-streptomycin, B27 supplement (Invitrogen, #17504–044). After 2 h media was changed to a fresh media containing 5% horse serum (Gibco, #26050–070) and 10 ng CTNF (Sino Biological, #11841-H-07E-5). Cells were maintained under 5% CO₂/10% O₂ atmosphere at 37°C for two days. The studies were conducted according to IACUC approved protocols at the UCR animal facility.

EphA4 Receptor Activation Assay—EphrinA1-Fc (R&D Systems, #602-A1) and human Fc (R&D Systems, #110-HG) were pre-clustered by the incubation with goat anti-human IgG (Jackson ImmunoResearch, #109–005-003) for 1 h at 4°C. At 2 days in vitro (DIV) primary motor neurons were treated with pre-clustered Fc (2 µg/mL), pre-clustered ephrinA1-Fc (2 µg/mL), APYd3, 123C4, compound **30**, compound **31**, compound **32** or **150D4** (at concentrations 1 µM and 10 µM) for 30 min at 37°C under 5% CO₂/10% O₂ atmosphere and then processed for western blotting. For growth cone analysis 2 DIV primary spinal cord motor neurons were treated as described above with Fc, ephrinA1-Fc, 1 µM **150D4**, 10 µM **150D4**, 1 µM **150D4** plus ephrinA1-Fc or 10 µM **150D4** plus ephrinA1-Fc. 0.1% DMSO was used as a negative control in both experiments.

Immunoprecipitation and Western Blot Analysis—Cells were collected and lysed in the lysis buffer (25 mM Tris-HCl, 150 mM NaCl, 5 mM EDTA, 1% Triton X-100, 1 mM sodium pervanadate, and protease inhibitor cocktail [1:100, Sigma, #P8340]) at 4°C for 30 min. Cell lysates were cleared by centrifugation at 13,500 rpm for 20 min at 4°C, then incubated with protein-A agarose beads (Sigma, #P1406) and anti-EphA4 antibody (Invitrogen, #371600), for 2 h at 4°C. Beads and cell lysate were boiled in reducing sample buffer (Laemmli 2× concentrate, Sigma, #S3401). Samples were briefly spun down and the supernatant was run on an 8%–16% Tris-glycine SDS-PAGE (Invitrogen, #XP08160BOX). Proteins were transferred onto Protran BA 85 nitrocellulose membrane (GE Healthcare) and blocked for 1 h at room temperature in 5% BSA. The blots were incubated with anti-phosphotyrosine antibody (BD Transduction, #610000) in Tris-buffered saline (TBS)/0.1% Tween 20/1% BSA at 4°C overnight. Membranes then were washed 3×10 min with TBS/0.1% Tween-20/1% BSA and incubated with HRP-conjugated anti-mouse secondary antibodies at 1:5000 (Jackson ImmunoResearch, #715–035-150) for 2 h at room temperature in a TBS/0.1% Tween-20/1% BSA solution. Blots were further incubated with ECL Detection reagent (Thermo Scientific, #32106) and imaged using ChemiDoc imaging system (Bio-Rad). For reprobing, membrane blots were washed in stripping buffer

(2% SDS, 100 mM β -mercaptoethanol, 50 mM Tris-HCl [pH 6.8]) for 30 min at 55°C and then washed 5×5 min with TBST, blocked with 5% skim milk, and re-probed for EphA4 (Invitrogen, #371600). Blots were washed 3×10 min with TBS/0.1% Tween 20 and then incubated with anti-mouse HRP-conjugated secondary antibodies in TBS/0.1% Tween 20/1% BSA (Jackson ImmunoResearch, #715–035-150) for 2 h at room temperature. After the incubation, blots were washed 3×10 min with TBS/0.1% Tween 20 and developed as described above. Blots with cell lysate samples were probed for ChAT (rabbit anti-mouse, Millipore-Sigma, #AB143, 1:1000) overnight and then incubated with corresponding secondary HRP-conjugated goat anti-rabbit antibody (Thermo Fisher Scientific, #G-21234) for 2 h as described above. Band density was analyzed by measuring band and background intensity using Adobe Photoshop CS5.1 software.

Immunocytochemistry—Primary neurons were fixed with 2% paraformaldehyde in 0.1 M PBS for 30 min at room temperature, then washed 3×10 min with 0.1 M PBS. Cells were permeabilized for 10 min at room temperature with 0.1% Triton X-100 in 0.1 M PBS and then washed 3×10 min in 0.1 M PBS. Cells were blocked with 5% NDS in 0.1 M PBS for 1 h at room temperature. For visualization of axon growth cones, cells were stained with phalloidin-rhodamine (1:40, Invitrogen, #R415) in a blocking buffer for 1 h at room temperature and motor neuron marker was immunolabeled with anti-ChAT antibody (1:500, Millipore-Sigma, #AB143) in 0.1 M PBS containing 1% NDS overnight at 4°C. Coverslips then were washed 3×10 min with 0.1 M PBS at room temperature followed by the incubation with Alexa Fluor 350-conjugated goat anti-rabbit immunoglobulin G (IgG) (1:500, Invitrogen, #A21068) for 2 h at room temperature. Coverslips were mounted on slides with Vectashield mounting medium (Vector Laboratories, #H100010).

Image Analysis—For growth cone analysis, images were captured using a Nikon Eclipse TE2000-U inverted fluorescent microscope with a 20×air objective and a Hamamatsu ORCA-AG 12-bit CCD camera using Image-Pro software. For analysis, 100 images were collected (2 coverslips/group, 3 experiments, 1–3 neurons/image) per treatment group. Growth cones were assessed based on filamentous (F)-actin labeling and classified into collapsed and growing based on their morphology. The percentage of neurons with collapsed growth cones was determined. Statistical differences for multiple groups were assessed by one-way ANOVA followed by Bonferroni's post hoc tests.

Co-culture Studies with Human Astrocytes and Motor Neurons—Patient fibroblasts were reprogrammed directly into neuronal progenitor cells (NPCs) as previously described.³⁰ Induced Astrocytes were generated by seeding a low quantity of NPCs into astrocyte medium (DMEM media containing 10% FBS and 0.2% N2) for five days. Following differentiation, iAstrocytes were lifted and seeded into a 96 well (10,000 cells per well).

Motor neurons expressing GFP under an HB9 promotor were differentiated from mouse embryonic bodies as previously described,³⁰ EBs were dissociated with papain and sorted using Becton-Dickenson Influx sorter using software. Cells are sorted through a 100 μ m tip with sheath pressure of 27. GFP+ motor neurons were seeded in a 96 well plate (10,000 cells

per well). Co-cultures were imaged with InCell for up to three days. Motor neurons with neurite outgrowth of greater than 50 μm were counted as alive.

Supplementary Material

Refer to Web version on PubMed Central for supplementary material.

Acknowledgments:

Financial support was obtained in part by NIH grants NS107479 (to MP, IE, and KM), CA168517 (to MP), CA242620 (to MP) and by Alcyone Therapeutics (to MP and KM). MP holds the Daniel Hays Chair in Cancer Research at the School of Medicine at UCR. Some molecular graphics and analyses performed with UCSF Chimera, developed by the Resource for Biocomputing, Visualization, and Informatics at the University of California, San Francisco, with support from NIH P41-GM103311.

Abbreviations used:

BAL	5-(4-Formyl-3,5-dimethoxyphenoxy)pentanoyl amido (4-methylphenyl)methyl polystyrene resin
DIPEA	N,N-Diisopropylethylamine
DMF	Dimethylformamide
HATU	1-[Bis(dimethylamino)methylene]-1H-1,2,3-triazolo[4,5-b]pyridinium 3-oxid hexafluorophosphate

References

1. Van Hoecke A; Schoonaert L; Lemmens R; Timmers M; Staats KA; Laird AS; Peeters E; Philips T; Goris A; Dubois B; Andersen PM; Al-Chalabi A; Thijs V; Turnley AM; van Vught PW; Veldink JH; Hardiman O; Van Den Bosch L; Gonzalez-Perez P; Van Damme P; Brown RH Jr.; van den Berg LH; Robberecht W, EphA4 Is a Disease Modifier of Amyotrophic Lateral Sclerosis in Animal Models and in Humans. *Nature medicine* 2012, 18 (9), 1418–1422.
2. Rue L; Oeckl P; Timmers M; Lenaerts A; van der Vos J; Smolders S; Poppe L; de Boer A; Van Den Bosch L; Van Damme P; Weishaupt JH; Ludolph AC; Otto M; Robberecht W; Lemmens R, Reduction of Ephrin-A5 Aggravates Disease Progression in Amyotrophic Lateral Sclerosis. *Acta Neuropathol Commun* 2019, 7 (1), 114. [PubMed: 31300041]
3. Wu B; De SK; Kulinich A; Salem AF; Koeppen J; Wang R; Barile E; Wang S; Zhang D; Ethell I; Pellecchia M, Potent and Selective EphA4 Agonists for the Treatment of ALS. *Cell Chem Biol* 2017, 24 (3), 293–305. [PubMed: 28196613]
4. Wu B; Barile E; De SK; Wei J; Purves A; Pellecchia M, High-Throughput Screening by Nuclear Magnetic Resonance (HTS by NMR) for the Identification of PPIs Antagonists. *Curr Top Med Chem* 2015, 15 (20), 2032–2042. [PubMed: 25986689]
5. Wu B; Zhang Z; Noberini R; Barile E; Giulianotti M; Pinilla C; Houghten RA; Pasquale EB; Pellecchia M, HTS by NMR of Combinatorial Libraries: A Fragment-Based Approach to Ligand Discovery. *Chemistry & biology* 2013, 20 (1), 19–33. [PubMed: 23352136]
6. Pinilla C; Appel JR; Blanc P; Houghten RA, Rapid Identification of High Affinity Peptide Ligands Using Positional Scanning Synthetic Peptide Combinatorial Libraries. *Biotechniques* 1992, 13 (6), 901–905. [PubMed: 1476743]
7. Barile E; Pellecchia M, Nmr-Based Approaches for the Identification and Optimization of Inhibitors of Protein-Protein Interactions. *Chem Rev* 2014, 114 (9), 4749–4763. [PubMed: 24712885]

8. Baggio C; Cerofolini L; Fragai M; Luchinat C; Pellecchia M, HTS by NMR for the Identification of Potent and Selective Inhibitors of Metalloenzymes. *ACS Med Chem Lett* 2018, 9 (2), 137–142. [PubMed: 29456802]
9. Baggio C; Velazquez JV; Fragai M; Nordgren TM; Pellecchia M, Therapeutic Targeting of Mmp-12 for the Treatment of Chronic Obstructive Pulmonary Disease. *J Med Chem* 2020, 63 (21), 12911–12920. [PubMed: 33107733]
10. Baggio C; Gambini L; Udompholkul P; Salem AF; Aronson A; Dona A; Troadec E; Pichiorri F; Pellecchia M, Design of Potent Pan-IAP and Lys-Covalent Xiap Selective Inhibitors Using a Thermodynamics Driven Approach. *J Med Chem* 2018, 61 (14), 6350–6363. [PubMed: 29940121]
11. Rue L; Timmers M; Lenaerts A; Smolders S; Poppe L; de Boer A; Van Den Bosch L; Van Damme P; Robberecht W; Lemmens R, Reducing Epha4 before Disease Onset Does Not Affect Survival in a Mouse Model of Amyotrophic Lateral Sclerosis. *Sci Rep* 2019, 9 (1), 14112. [PubMed: 31575928]
12. Murai KK; Nguyen LN; Koolpe M; McLennan R; Krull CE; Pasquale EB, Targeting the Epha4 Receptor in the Nervous System with Biologically Active Peptides. *Molecular and cellular neurosciences* 2003, 24 (4), 1000–1011. [PubMed: 14697664]
13. Noberini R; Koolpe M; Peddibhotla S; Dahl R; Su Y; Cosford ND; Roth GP; Pasquale EB, Small Molecules Can Selectively Inhibit Ephrin Binding to the EphA4 and EphA2 Receptors. *The Journal of biological chemistry* 2008, 283 (43), 29461–29472. [PubMed: 18728010]
14. Tognolini M; Incerti M; Lodola A, Are We Using the Right Pharmacological Tools to Target EphA4? *ACS Chem Neurosci* 2014, 5 (12), 1146–1147. [PubMed: 25405504]
15. Noberini R; De SK; Zhang Z; Wu B; Raveendra-Panickar D; Chen V; Vazquez J; Qin H; Song J; Cosford ND; Pellecchia M; Pasquale EB, A Disalicylic Acid-Furanyl Derivative Inhibits Ephrin Binding to a Subset of Eph Receptors. *Chem Biol Drug Des* 2011, 78 (4), 667–678. [PubMed: 21791013]
16. Olson EJ; Lechtenberg BC; Zhao C; Rubio de la Torre E; Lamberto I; Riedl SJ; Dawson PE; Pasquale EB, Modifications of a Nanomolar Cyclic Peptide Antagonist for the EphA4 Receptor to Achieve High Plasma Stability. *ACS Med Chem Lett* 2016, 7 (9), 841–846. [PubMed: 27660688]
17. Zhao J; Cooper LT; Boyd AW; Bartlett PF, Decreased Signalling of Epha4 Improves Functional Performance and Motor Neuron Survival in the SOD1(G93A) ALS Mouse Model. *Sci Rep* 2018, 8 (1), 11393. [PubMed: 30061574]
18. Pasquale EB, Eph-Ephrin Bidirectional Signaling in Physiology and Disease. *Cell* 2008, 133 (1), 38–52. [PubMed: 18394988]
19. Furne C; Ricard J; Cabrera JR; Pays L; Bethea JR; Mehlen P; Liebl DJ, Ephrinb3 Is an Anti-Apoptotic Ligand That Inhibits the Dependence Receptor Functions of EphA4 Receptors During Adult Neurogenesis. *Biochim Biophys Acta* 2009, 1793 (2), 231–238. [PubMed: 18948148]
20. Baggio C; Udompholkul P; Barile E; Pellecchia M, Enthalpy-Based Screening of Focused Combinatorial Libraries for the Identification of Potent and Selective Ligands. *ACS Chem Biol* 2017, 12 (12), 2981–2989. [PubMed: 29094589]
21. Ran X; Gestwicki JE, Inhibitors of Protein-Protein Interactions (PPIs): An Analysis of Scaffold Choices and Buried Surface Area. *Curr Opin Chem Biol* 2018, 44, 75–86. [PubMed: 29908451]
22. Bowden TA; Aricescu AR; Nettleship JE; Siebold C; Rahman-Huq N; Owens RJ; Stuart DI; Jones EY, Structural Plasticity of Eph Receptor A4 Facilitates Cross-Class Ephrin Signaling. *Structure* 2009, 17 (10), 1386–1397. [PubMed: 19836338]
23. Forse GJ; Uson ML; Nasertorabi F; Kolatkar A; Lamberto I; Pasquale EB; Kuhn P, Distinctive Structure of the EphA3/Ephrin-A5 Complex Reveals a Dual Mode of Eph Receptor Interaction for Ephrin-A5. *PLoS One* 2015, 10 (5), e0127081. [PubMed: 25993310]
24. Di Giorgio FP; Carrasco MA; Siao MC; Maniatis T; Eggan K, Non-Cell Autonomous Effect of Glia on Motor Neurons in an Embryonic Stem Cell-Based ALS Model. *Nat Neurosci* 2007, 10 (5), 608–614. [PubMed: 17435754]
25. Nagai M; Re DB; Nagata T; Chalazonitis A; Jessell TM; Wichterle H; Przedborski S, Astrocytes Expressing Als-Linked Mutated SOD1 Release Factors Selectively Toxic to Motor Neurons. *Nat Neurosci* 2007, 10 (5), 615–622. [PubMed: 17435755]

26. Yamanaka K; Chun SJ; Boillee S; Fujimori-Tonou N; Yamashita H; Gutmann DH; Takahashi R; Misawa H; Cleveland DW, Astrocytes as Determinants of Disease Progression in Inherited Amyotrophic Lateral Sclerosis. *Nat Neurosci* 2008, 11 (3), 251–253. [PubMed: 18246065]
27. Di Giorgio FP; Boulting GL; Bobrowicz S; Eggan KC, Human Embryonic Stem Cell-Derived Motor Neurons Are Sensitive to the Toxic Effect of Glial Cells Carrying an Als-Causing Mutation. *Cell Stem Cell* 2008, 3 (6), 637–648. [PubMed: 19041780]
28. Marchetto MC; Muotri AR; Mu Y; Smith AM; Cezar GG; Gage FH, Non-Cell-Autonomous Effect of Human SOD1 G37R Astrocytes on Motor Neurons Derived from Human Embryonic Stem Cells. *Cell Stem Cell* 2008, 3 (6), 649–657. [PubMed: 19041781]
29. Haidet-Phillips AM; Hester ME; Miranda CJ; Meyer K; Braun L; Frakes A; Song S; Likhite S; Murtha MJ; Foust KD; Rao M; Eagle A; Kammesheidt A; Christensen A; Mendell JR; Burghes AH; Kaspar BK, Astrocytes from Familial and Sporadic ALS Patients Are Toxic to Motor Neurons. *Nat Biotechnol* 2011, 29 (9), 824–828. [PubMed: 21832997]
30. Meyer K; Ferraiuolo L; Miranda CJ; Likhite S; McElroy S; Renusch S; Ditsworth D; Lagier-Tourenne C; Smith RA; Ravits J; Burghes AH; Shaw PJ; Cleveland DW; Kolb SJ; Kaspar BK, Direct Conversion of Patient Fibroblasts Demonstrates Non-Cell Autonomous Toxicity of Astrocytes to Motor Neurons in Familial and Sporadic Als. *Proc Natl Acad Sci U S A* 2014, 111 (2), 829–832. [PubMed: 24379375]
31. Boyd AW; Bartlett PF; Lackmann M, Therapeutic Targeting of Eph Receptors and Their Ligands. *Nat Rev Drug Discov* 2014, 13 (1), 39–62. [PubMed: 24378802]
32. Lamberto I; Qin H; Noberini R; Premkumar L; Bourgin C; Riedl SJ; Song J; Pasquale EB, Distinctive Binding of Three Antagonistic Peptides to the Ephrin-Binding Pocket of the EphA4 Receptor. *The Biochemical journal* 2012, 445 (1), 47–56. [PubMed: 22489865]
33. Lamberto I; Lechtenberg BC; Olson EJ; Mace PD; Dawson PE; Riedl SJ; Pasquale EB, Development and Structural Analysis of a Nanomolar Cyclic Peptide Antagonist for the EphA4 Receptor. *ACS chemical biology* 2014, 9 (12), 2787–2795. [PubMed: 25268696]
34. Xu K; Tzvetkova-Robev D; Xu Y; Goldgur Y; Chan YP; Himanen JP; Nikolov DB, Insights into Eph Receptor Tyrosine Kinase Activation from Crystal Structures of the EphA4 Ectodomain and Its Complex with Ephrin-A5. *Proc Natl Acad Sci U S A* 2013, 110 (36), 14634–14639. [PubMed: 23959867]
35. Li JJ; Liu DP; Liu GT; Xie D, Ephrina5 Acts as a Tumor Suppressor in Glioma by Negative Regulation of Epidermal Growth Factor Receptor. *Oncogene* 2009, 28 (15), 1759–1768. [PubMed: 19270726]
36. Pensold D; Gehrman J; Pitschelatow G; Walberg A; Braunsteffer K; Reichard J; Ravaei A; Linde J; Lampert A; Costa IG; Zimmer-Bensch G, The Expression of the Cancer-Associated Lncrna Snhg15 Is Modulated by EphrinA5-Induced Signaling. *Int J Mol Sci* 2021, 22 (3).
37. Wang TH; Chang JL; Ho JY; Wu HC; Chen TC, Ephrina5 Suppresses Colon Cancer Development by Negatively Regulating Epidermal Growth Factor Receptor Stability. *FEBS J* 2012, 279 (2), 251–263. [PubMed: 22074469]
38. Fu AK; Hung KW; Huang H; Gu S; Shen Y; Cheng EY; Ip FC; Huang X; Fu WY; Ip NY, Blockade of EphA4 Signaling Ameliorates Hippocampal Synaptic Dysfunctions in Mouse Models of Alzheimer’s Disease. *Proceedings of the National Academy of Sciences of the United States of America* 2014, 111 (27), 9959–9964. [PubMed: 24958880]
39. Spanevello MD; Tajouri SI; Mirciov C; Kurniawan N; Pearse MJ; Fabri LJ; Owczarek CM; Hardy MP; Bradford RA; Ramunno ML; Turnley AM; Ruitenber MJ; Boyd AW; Bartlett PF, Acute Delivery of EphA4-Fc Improves Functional Recovery after Contusive Spinal Cord Injury in Rats. *J Neurotrauma* 2013, 30 (12), 1023–1034. [PubMed: 23557244]
40. Hanell A; Clausen F; Djupsjo A; Vallstedt A; Patra K; Israelsson C; Larhammar M; Bjork M; Paixao S; Kullander K; Marklund N, Functional and Histological Outcome after Focal Traumatic Brain Injury Is Not Improved in Conditional EphA4 Knockout Mice. *J Neurotrauma* 2012, 29 (17), 2660–2671. [PubMed: 22985250]
41. Frugier T; Conquest A; McLean C; Currie P; Moses D; Goldshmit Y, Expression and Activation of EphA4 in the Human Brain after Traumatic Injury. *J Neuropathol Exp Neurol* 2012, 71 (3), 242–250. [PubMed: 22318127]

42. Fukai J; Yokote H; Yamanaka R; Arao T; Nishio K; Itakura T, EphA4 Promotes Cell Proliferation and Migration through a Novel EphA4-Fgfr1 Signaling Pathway in the Human Glioma U251 Cell Line. *Mol Cancer Ther* 2008, 7 (9), 2768–2778. [PubMed: 18790757]
43. Miyazaki K; Inokuchi M; Takagi Y; Kato K; Kojima K; Sugihara K, EphA4 Is a Prognostic Factor in Gastric Cancer. *BMC Clin Pathol* 2013, 13 (1), 19. [PubMed: 23738943]
44. Oshima T; Akaike M; Yoshihara K; Shiozawa M; Yamamoto N; Sato T; Akihito N; Nagano Y; Fujii S; Kunisaki C; Wada N; Rino Y; Tanaka K; Masuda M; Imada T, Overexpression of EphA4 Gene and Reduced Expression of EphB2 Gene Correlates with Liver Metastasis in Colorectal Cancer. *Int J Oncol* 2008, 33 (3), 573–577. [PubMed: 18695888]
45. Iizumi M; Hosokawa M; Takehara A; Chung S; Nakamura T; Katagiri T; Eguchi H; Ohigashi H; Ishikawa O; Nakamura Y; Nakagawa H, EphA4 Receptor, Overexpressed in Pancreatic Ductal Adenocarcinoma, Promotes Cancer Cell Growth. *Cancer Sci* 2006, 97 (11), 1211–1216. [PubMed: 16965393]

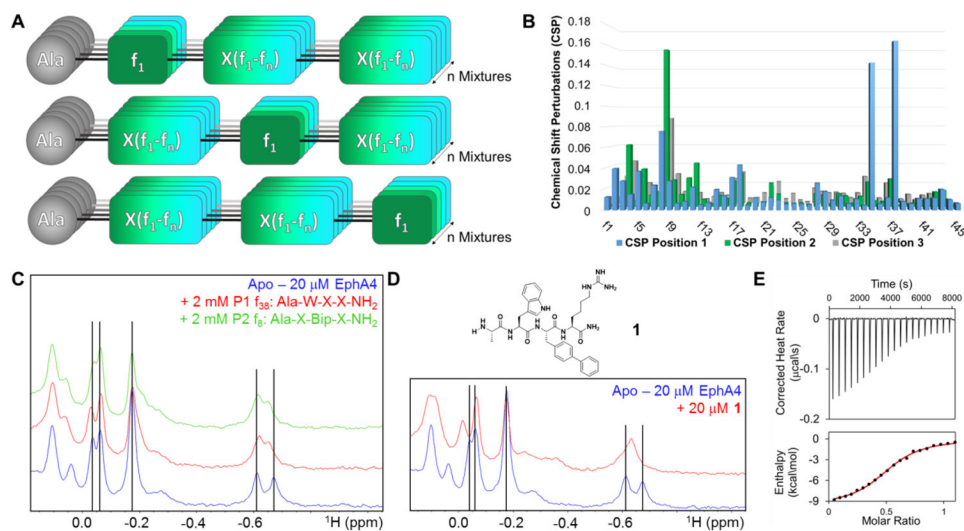


Figure 1. HTS by NMR summary as deployed against EphA4-LBD. **A)** Schematic representation of the Ala-XXX positional scanning library made up by 46×3 mixtures each containing 46×46 tetrapeptides. **B)** Summary of the chemical shift perturbations induced by each mixture. The perturbations were detected using 1D ^1H aliphatic region of the EphA4-LBD as illustrated in panel C). **D)** Chemical structure of consensus agent **1** and relative perturbations induced (at 20 μM) in the 1D ^1H aliphatic spectrum of EphA4 (20 μM). **E)** ITC data with EphA4-LBD and compound **1**. Fitting of the titration points resulted in a dissociation constant for the complex $K_d \sim 3 \mu\text{M}$.

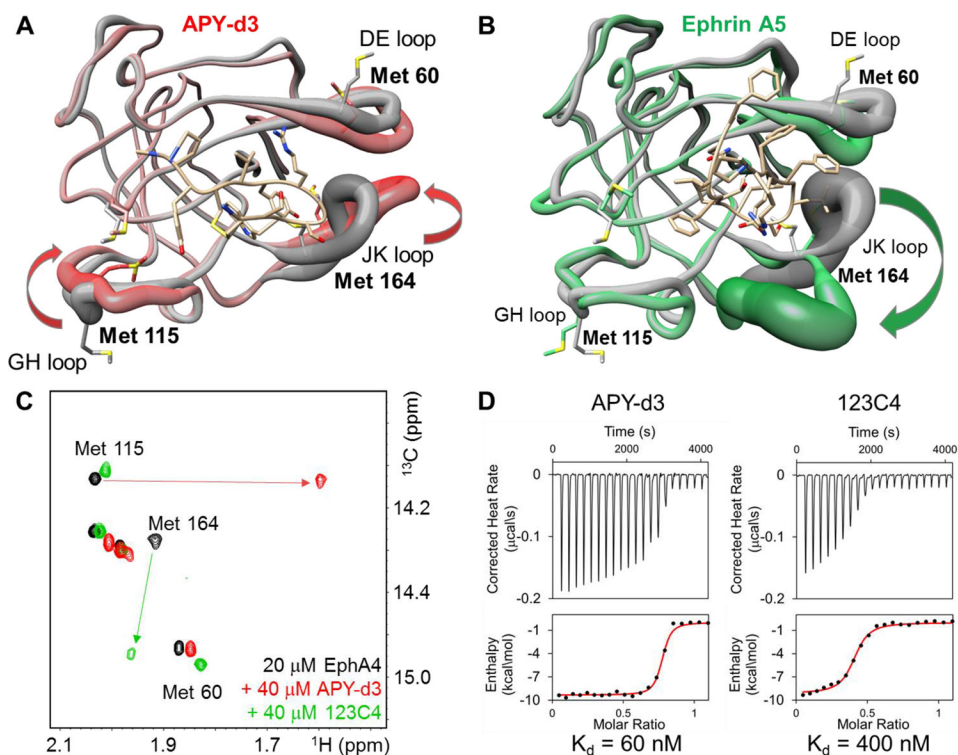


Figure 2. Biophysical studies on EphA4-LBD in the free versus bound state. **A)** Superposition of the X-ray structures of EphA4-LBD in the apo form (PDB ID 2WO1; gray) and APY-d3 bound (PDB ID 5JR2; red and stick model for APY-d3). The thickness of the tube is proportional to the pairwise backbone C α atoms RMSD between the two compared structures. Most notable conformational changes upon antagonist APY-d3 binding are highlighted, together with Met residues that are displayed as stick models. **B)** Superposition of the X-ray structures of EphA4-LBD in the apo form (PDB ID 2WO1; gray) and ephrinA5 bound (PDB ID 4BKA; green and stick model showing only a peptide region from ephrinA5 that is contact with the EphA4-LBD). Most notable conformational changes upon agonist ephrinA5 binding are highlighted, together with Met residues. **C)** 2D [^{13}C , ^1H] correlation spectra for EphA4-LBD $^{13}\text{C}^e$ -Met labeled, measured in absence and in presence of antagonist APY-d3 or agonist 123C4. **D)** ITC curves for the binding of agents APY-d3 or 123C4 to EphA4-LBD.

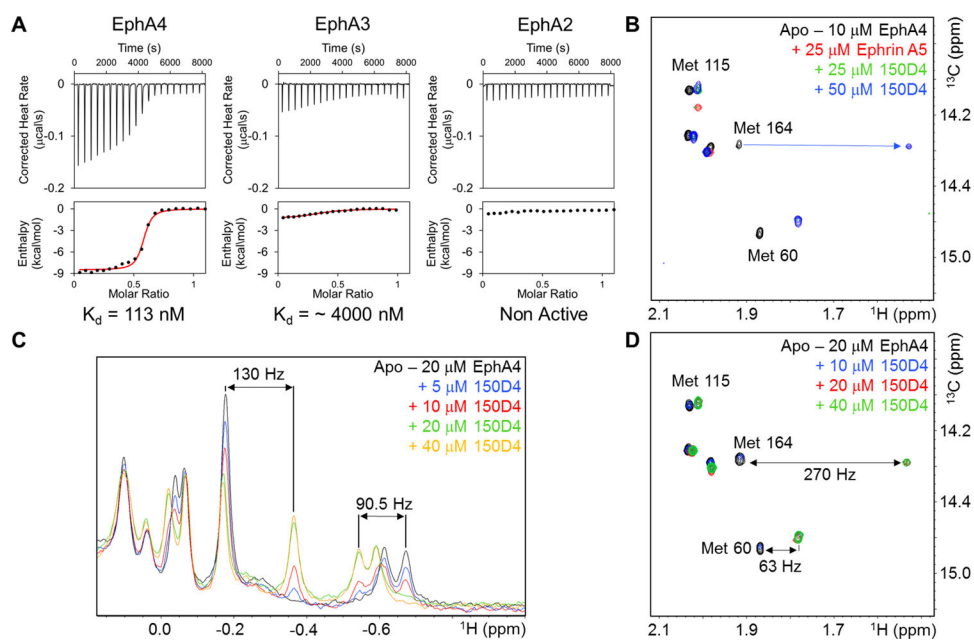


Figure 3. Biophysical characterizations of **150D4** binding to EphA4-LBD. **A)** ITC data for the binding of **150D4** to EphA4-LBD, EphA3-LBD, or EphA2-LBD. **B)** **150D4** displaces the binding between EphA4-LBD and ephrinA5, as detected by [^{13}C , ^1H] correlation spectra with EphA4-LBD ^{13}C -Met. **C)** and **D)** report 1D ^1H NMR and 2D [^{13}C , ^1H] correlation spectra, respectively, of ^{13}C -Met-EphA4-LBD recorded in presence of various concentrations of **150D4**.

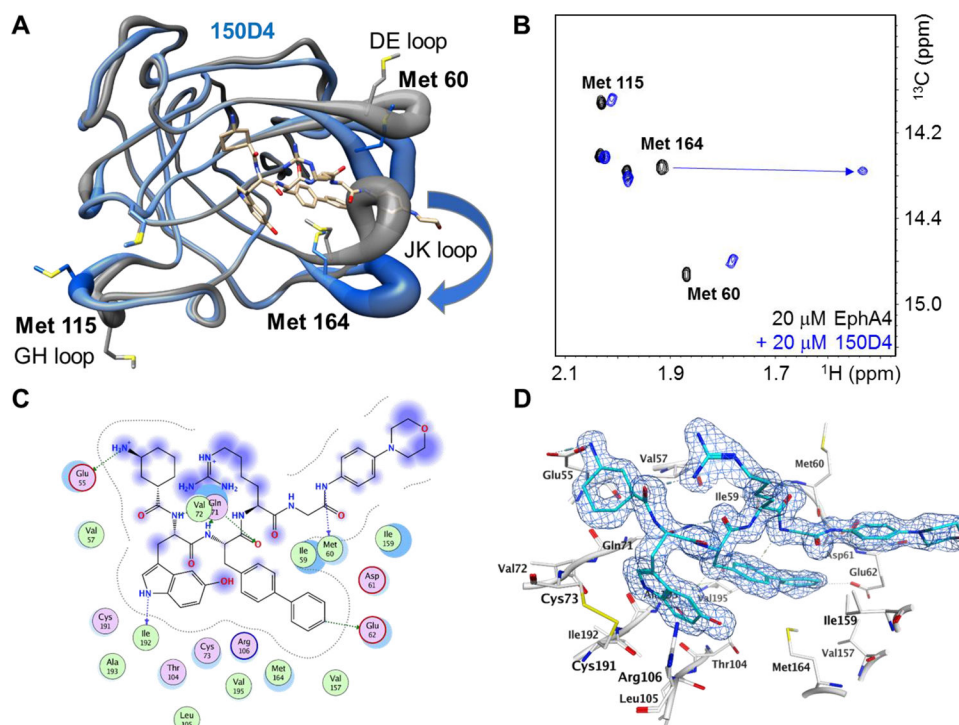


Figure 4. X-ray and NMR studies with **150D4** in complex with EphA4-LBD. **A)** Superposition of the structure of EphA4-LBD in complex with **150D4** (blue and sticks model; PDB ID 7OFV) versus the apo structure of EphA4-LBD (PDB ID 2WO1). The highlighted conformational changes are similar to those induced by the agonistic ligand ephrinA5 (see Figure 2). **B)** 2D [^{13}C , ^1H] correlation spectra of $^{13}\text{C}^{\text{e}}$ -Met-EphA4-LBD collected in absence and presence of **150D4**. The large chemical shift changes for residues Met 60 and Met 164 induced by **150D4** are in agreement with the conformational changes observed in loops D-E and J-K, respectively, while and unlike APY-d3, no significant perturbations were observed for Met 115, in the G-H loop. **C)** Schematic plot to represent the intermolecular interactions between **150D4** and EphA4-LBD. **D)** Stick model and contour map of the observed electron density for **150D4** when in complex with EphA4-LBD (PDB ID 7OFV). The ligand molecule is shown superimposed with the refined 2Fo-Fc electron density map contoured at 1.0σ .

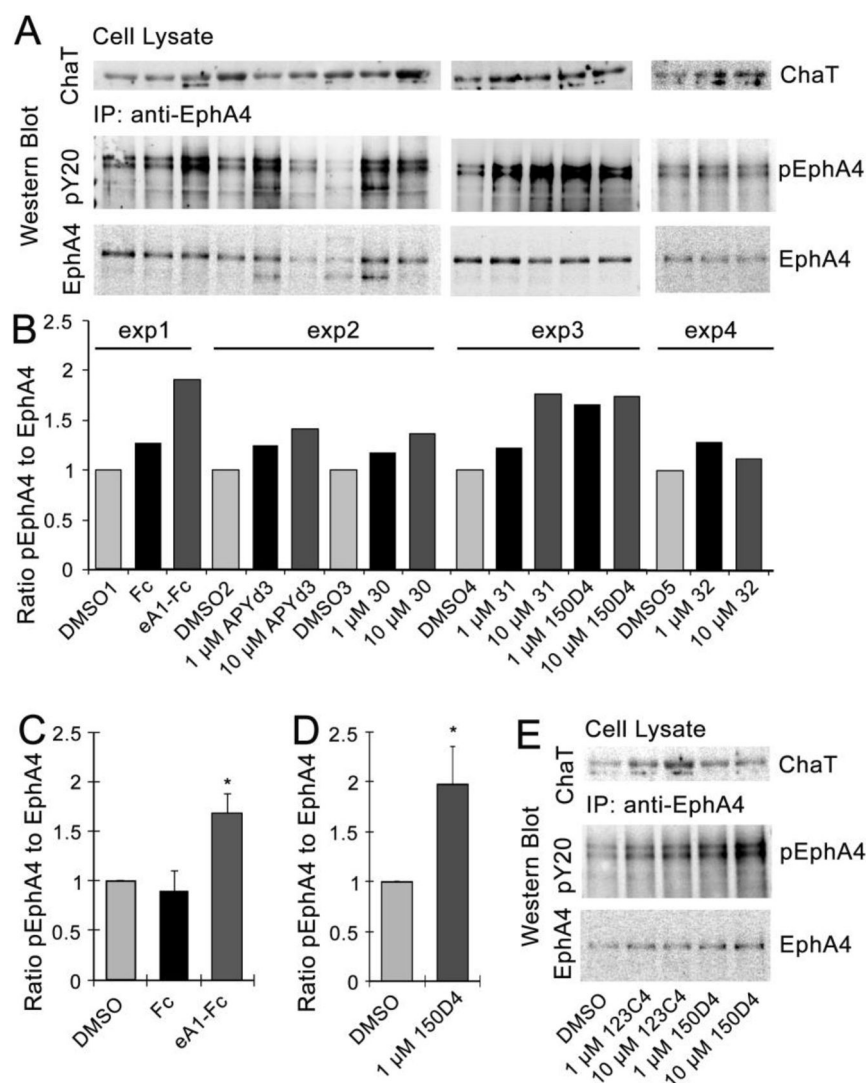


Figure 5. EphA4 phosphorylation in primary spinal cord motor neurons.

A) Representative western blot images of pEphA4, total EphA4 (after immunoprecipitation, IP) and a motor neuron marker, choline acetyltransferase (ChAT, in cell lysate) in cultures of primary spinal cord motor neurons treated with DMSO, Fc, ephrinA1-Fc (eA1-Fc), APYd3, **30**, **31**, **32**, and **150D4** (1 μ M and 10 μ M) for 30 min. **B-D)** Graphs show average ratio of pEphA4 and total EphA4 in primary motor neuron cultures treated with DMSO, Fc, eA1-Fc, APYd3, **30**, **31**, **32**, and **150D4** (**B**); DMSO, Fc and eA1-Fc (**C**); DMSO and 1 μ M **150D4** (**D**). Black solid lines above the graph indicate separate experiments (experiments 1–4, **B**). Error bars indicate SEM (each experiment was repeated 3 times). Statistical analysis was performed using one-way ANOVA followed by Bonferroni's post-hoc analysis (* $p < 0.05$, **C**) or two-tailed, unpaired student's *t* test for comparison of two groups; * $p < 0.05$ ($p=0.035$, **D**). **E**, representative western blot images of pEphA4, total EphA4 and ChAT in primary spinal cord motor neurons treated with DMSO, 1 μ M 123C3, 10 μ M 123C4, 1 μ M **150D4**, or 10 μ M **150D4**. WB images that generated the panels C and D are reported as supplementary Figure S9.

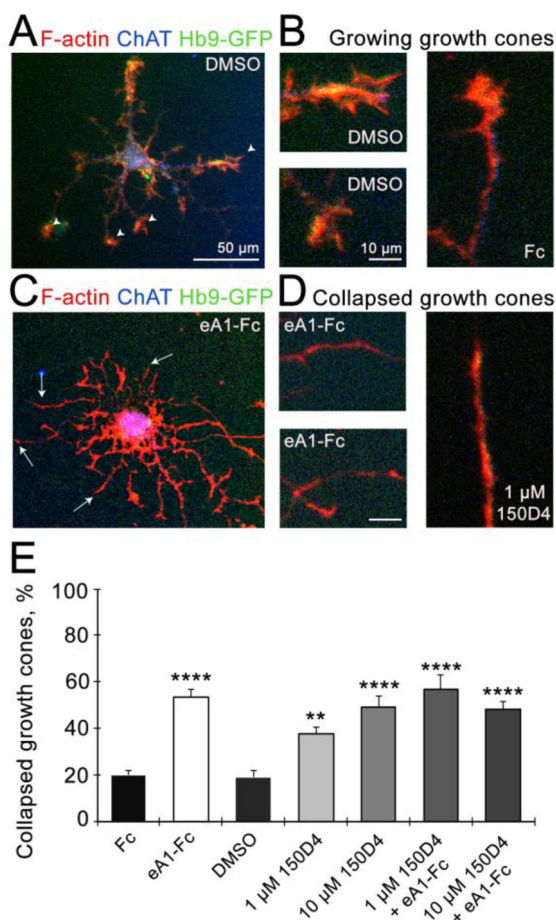


Figure 6. Growth cone collapse in primary spinal cord motor neurons. A-D, Representative images of 2 DIV primary spinal cord motor neurons treated with DMSO (A), Fc (Fc), eA1-Fc (C), 1 μ M **150D4** or 10 μ M **150D4**. Growth cone morphology was assessed by labeling F-actin with rhodamine-coupled phalloidin (red). Motor neurons were identified by genetically encoded Hb9-GFP (green) and immunostaining against ChAT (blue). (B, D) High magnification images of growing (B) and collapsed (D) growth cones. Scale bars are 50 μ m in A, C and 10 μ m in B, D. (E) Graph shows average percent of collapsed growth cones in primary spinal cord motor neuron cultures treated with DMSO, Fc (Fc), eA1-Fc, 1 μ M **150D4**, 10 μ M **150D4**, 1 μ M **150D4** plus ephrin A1-Fc or 10 μ M **150D4** plus ephrin A1-Fc. Error bars indicate SEM (n=4–6 coverslips). Statistical analysis was performed using one-way ANOVA followed by Bonferroni's post-hoc analysis (** $p < 0.01$, **** $p < 0.0001$).

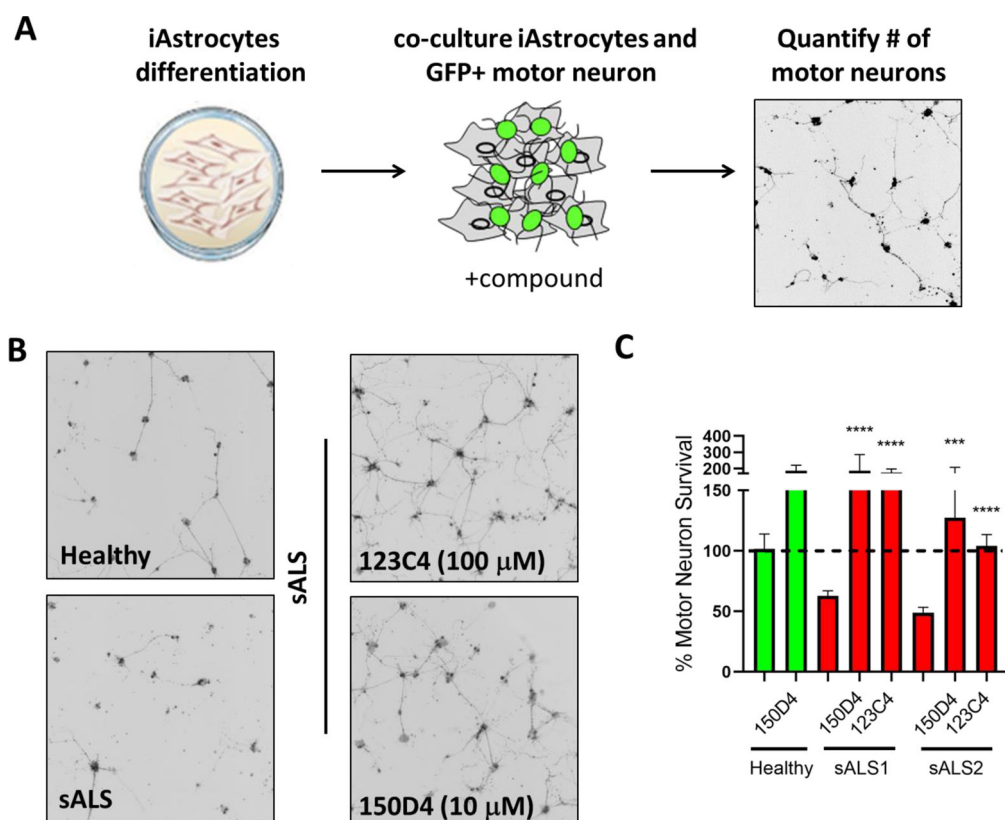


Figure 7.

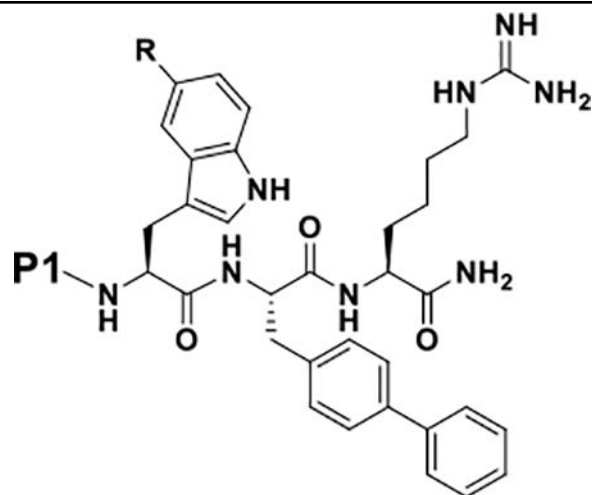
EphA4 agonists protects from iAstrocyte mediated motor neuron death at lower concentrations. **A)** Schematic illustration of the assay. NPCs were differentiated into induced astrocytes for five days then seeded on a 96 well plate. 10 μM of new ephrin ligand compounds were added 24 hours later at the time of motor neuron addition. 100 μM 123C4 was added to co-culture at time of motor neuron addition as a positive control. **B)** Representative image of motor neurons (black) following 3 days in co-culture. **C)** Quantification of motor neuron survival following co-culture. Data was normalized to average motor neuron survival of healthy controls. Data represents a minimum of 2 independent experiments.

Statistical analysis was performed using unpaired t-test comparing corresponding treated and untreated iAs.

Table 1.

Compound ID, chemical structures and binding properties of EphA4 targeting agents.

ID	P1	R	K_d [nM]	H [kcal/mol]	-T S [kcal/mol]	$\delta^{13}\text{C}^\epsilon/\text{H}^\epsilon$ Met 164
1		-H	3022	-9.54	2.01	-
2		-H	2130	-11.50	3.77	+
3		-H	663	-10.70	2.27	+
4		-OH	352	-11.59	2.79	+
5		-OH	1211	-9.39	1.32	-
6		-OH	370	-8.10	-0.67	++

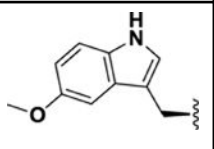
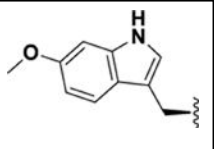
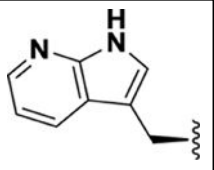


ID	P1	R	K_d [nM]	H [kcal/mol]	$-T \Delta S$ [kcal/mol]	$\delta^{13C^e/1H^e}$ Met 164
7		-OH	740	-9.82	1.46	-
8		-OH	1117	-8.33	0.21	-

K_d and thermodynamic binding parameters were obtained by isothermal titration calorimetry measurements against recombinant EphA4 ligand binding domain. δ indicates chemical shift perturbations induced by test ligands (at 40 μ M concentration) to $^1H^e/^{13}C^e$ resonances of Met164 in EphA4-LDB (at 20 μ M). δ values represent weight average perturbations observed in the 1H and ^{13}C dimensions, as described in the methods. δ : -, no changes; 0 < + < 0.1 ppm; 0.1 ppm < ++ < 0.2 ppm; 0.2 < +++ < 0.25; ++++ > 0.25 ppm.

Table 2.

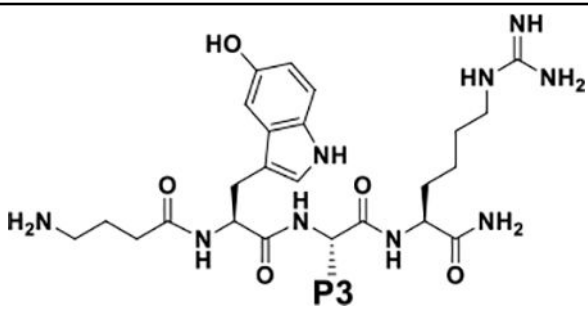
Compound ID, chemical structures and binding properties of EphA4 targeting agents.

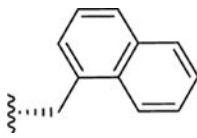
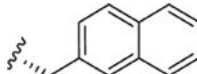
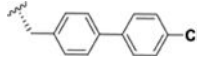
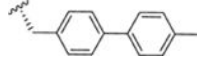
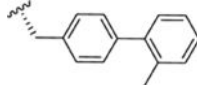
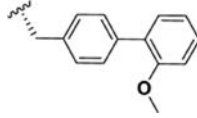
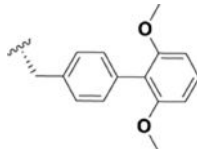
ID	P2	K_d [nM]	H [kcal/mol]	-T S [kcal/mol]	δ $^{13}\text{C}/^1\text{H}^e$ Met 164
9		444	-10.56	1.90	+
10		2463	-10.49	2.84	-
11		16280	-7.27	0.74	-

K_d and thermodynamic binding parameters were obtained by isothermal titration calorimetry measurements against recombinant EphA4 ligand binding domain. δ indicates chemical shift perturbations induced by test ligands (at 40 μM concentration) to $^1\text{H}^e/^{13}\text{C}^e$ resonances of Met 164 in EphA4-LDB (at 20 μM). δ values represent weight average perturbations observed in the ^1H and ^{13}C dimensions, as described in the methods. δ : -, no changes; $0 < + < 0.1$ ppm; 0.1 ppm $< ++ < 0.2$ ppm; $0.2 < +++ < 0.25$; $+++ > 0.25$ ppm.

Table 3.

Compound ID, chemical structures and binding properties of EphA4 targeting agents.

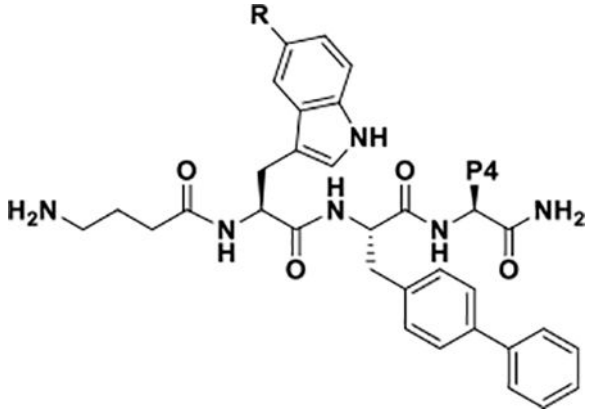


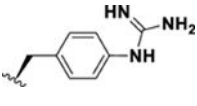
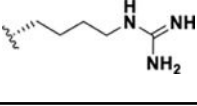
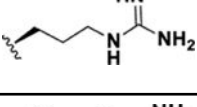

ID	P3	K_d [nM]	H [kcal/mol]	-T S [kcal/mol]	$\delta^{13}\text{C}^e/{}^1\text{H}^e$ Met 164
12		11050	-8.22	1.46	-
13		5250	-8.49	1.27	-
14		749	-10.36	2.00	++
15		708	-10.16	1.77	-
16		362	-12.08	3.29	+
17		196	-12.29	3.14	++
18		1094	-10.73	2.60	-

K_d and thermodynamic binding parameters were obtained by isothermal titration calorimetry measurements against recombinant EphA4 ligand binding domain. δ indicates chemical shift perturbations induced by test ligands (at 40 μM concentration) to ${}^1\text{H}^e/{}^{13}\text{C}^e$ resonances of Met 164 in EphA4-LDB (at 20 μM). δ values represent weight average perturbations observed in the ${}^1\text{H}$ and ${}^{13}\text{C}$ dimensions, as described in the methods. δ : -, no changes; $0 < + < 0.1$ ppm; 0.1 ppm $< ++ < 0.2$ ppm; $0.2 < +++ < 0.25$; $+++ > 0.25$ ppm.

Table 4.

Compound ID, chemical structures and binding properties of EphA4 targeting agents.

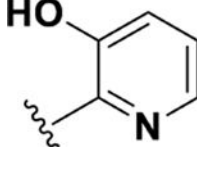
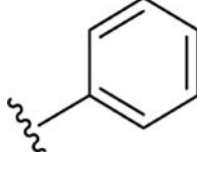
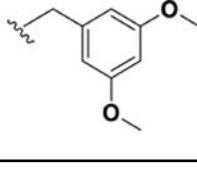
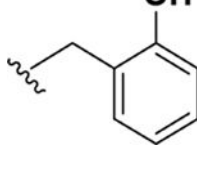
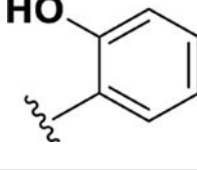
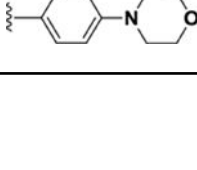


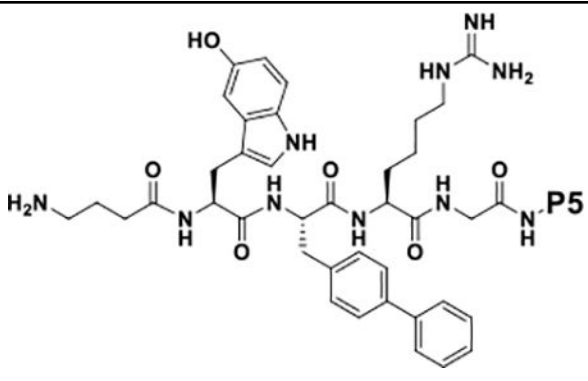
ID	P4	R	K_d [nM]	H [kcal/mol]	-T S [kcal/mol]	NMR $^{13}\text{C}/^1\text{H}^e$ Met164
19		-H	1156	-9.43	1.33	-
20		-H	270	-9.26	0.30	-
21		-OH	459	-10.99	2.35	+
22		-OH	437	-11.21	2.54	+

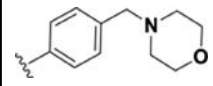
K_d and thermodynamic binding parameters were obtained by isothermal titration calorimetry measurements against recombinant EphA4 ligand binding domains. δ indicates chemical shift perturbations induced by test ligands (at 40 μM concentration) to $^1\text{H}^e/^{13}\text{C}^e$ resonances of Met 164 in EphA4-LDB (at 20 μM). δ values represent weight average perturbations observed in the ^1H and ^{13}C dimensions, as described in the methods. δ : -, no changes; 0 < + < 0.1 ppm; 0.1 ppm < ++ < 0.2 ppm; 0.2 < +++ < 0.25; ++++ > 0.25 ppm.

Table 5.

Compound ID, chemical structures and binding properties of EphA4 targeting agents.

ID	P5	K_d [nM]	H [kcal/mol]	-T S [kcal/mol]	$\delta^{13}\text{C}^e/{}^1\text{H}^e$ Met 164
23		488	-9.48	0.86	+
24		132	-12.26	2.87	++
25		307	-11.27	2.39	+
26		258	-11.98	3.00	+
27		191	-12.04	2.88	++
28		94	-11.22	1.63	++++

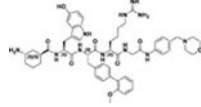
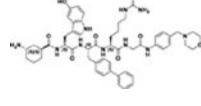
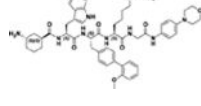
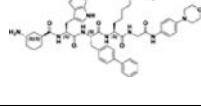
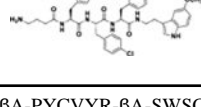


ID	P5	K_d [nM]	H [kcal/mol]	-T S [kcal/mol]	δ $^{13}\text{C}^e/{}^1\text{H}^e$ Met 164
29		106	-10.56	1.05	+++

K_d and thermodynamic binding parameters were obtained by isothermal titration calorimetry measurements against recombinant EphA4 ligand binding domains. δ indicates chemical shift perturbations induced by test ligands (at 40 μM concentration) to ${}^1\text{H}^e/{}^{13}\text{C}^e$ resonances of Met 164 in EphA4-LDB (at 20 μM). δ values represent weight average perturbations observed in the ${}^1\text{H}$ and ${}^{13}\text{C}$ dimensions, as described in the methods. δ : -, no changes; $0 < + < 0.1$ ppm; 0.1 ppm $< ++ < 0.2$ ppm; $0.2 < +++ < 0.25$; $+++ > 0.25$ ppm.

Table 6.

Compound ID, chemical structures, and binding properties of EphA4 targeting agents.

ID	Structure	MW	K_d (nM) vs EphA4	K_d (nM) vs EphA3	K_d (nM) vs EphA2	Aqueous Solubility	δ Met 164	δ Met 115	δ Met 60
30		1000	77	~9000	N.A.	> 50 mM	+	+	++
31		970	144	~7000	N.A.	> 50 mM	+++	+	++
32		986	106	~7000	N.A.	> 50 mM	+	+	+
33 (150D4)		956	113	~4000	N.A.	> 50 mM	++++	+	++
123C4		807	400	>10000	N.A.	~100 μ M	++	+	+
APY-d3	β A-PYCVYR- β A-SWSC- CONH ₂	1402	60	~1500	N.D.	N.D.	+	++++	+

K_d values were obtained by isothermal titration calorimetry measurements with the respective ligand binding domains. δ indicate chemical shift perturbations induced by test ligands (at 40 μ M concentration) to $^1\text{H}/^{13}\text{C}$ resonances of the indicated residues in EphA4-LDB (at 20 μ M). δ values represent weight average perturbations observed in the ^1H and ^{13}C dimensions, as described in the methods. δ : -, no changes; $0 < + < 0.1$ ppm; $0.1 \text{ ppm} < ++ < 0.2$ ppm; $0.2 < +++ < 0.25$; $+++ > 0.25$ ppm. N.D., not determined; N.A., no affinity detectable under the tested experimental conditions.